AD-A214 340

AFIT/GEO/ENG/89D-3

NEURAL NETWORK ASSOCIATIVE MEMORY USING NON-LINEAR HOLOGRAPHIC STORAGE MEDIA

THESIS

Presented to the Faculty of the School of Engineering
of the Air Force Institute of Technology
Air University
In Partial Fulfillment of the
Requirements for the Degree of
Master of Science in Electrical Engineering

Dwayne William Frye, B.S.E.E., M.B.A.
Captain, USAF

December, 1989

Approved for public release; distribution unlimited

UNCLASSIFIED
SECURITY CLASSIFICATION OF THIS PAGE

REPORT DOCUMENTATION PAGE

Form Approved
OMB No. 0704-0188

1a. REPORT SECURITY CLASSIFICATION UNCLASSIFIED	1b. RESTRICTIVE MARKINGS
2a. SECURITY CLASSIFICATION AUTHORITY	3. DISTRIBUTION / AVAILABILITY OF REPORT Approved for public release; distribution unlimited
2b. DECLASSIFICATION / DOWNGRADING SCHEDULE	
4. PERFORMING ORGANIZATION REPORT NUMBER(S) AFIT/GEC/ENG/89D-3	5. MONITORING ORGANIZATION REPORT NUMBER(S)
6a. NAME OF PERFORMING ORGANIZATION School of Engineering 6b. OFFICE SYMBOL (If applicable) AFIT/ENG	7a. NAME OF MONITORING ORGANIZATION
6c. ADDRESS (City, State, and ZIP Code) Air Force Institute of Technology (AU) Wright-Patterson AFB, OH 45433-6583	7b. ADDRESS (City, State, and ZIP Code)
8a. NAME OF FUNDING / SPONSORING ORGANIZATION Rome Air Development Cen. 8b. OFFICE SYMBOL (If applicable) RADC/OPB	9. PROCUREMENT INSTRUMENT IDENTIFICATION NUMBER
8c. ADDRESS (City, State, and ZIP Code) Griffiss AFB, NY 13441	10. SOURCE OF FUNDING NUMBERS PROGRAM ELEMENT NO. / PROJECT NO. / TASK NO / WORK UNIT ACCESSION NO.

11. TITLE (Include Security Classification)

NEURAL NETWORK ASSOCIATIVE MEMORY USING NON-LINEAR HOLOGRAPHIC STORAGE MEDIA

12. PERSONAL AUTHOR(S)
Dwayne William Frye, Capt, USAF

13a. TYPE OF REPORT	13b. TIME COVERED	14. DATE OF REPORT (Year, Month, Day)	15. PAGE COUNT
MS Thesis	FROM _____ TO _____	1989 December	86

16. SUPPLEMENTARY NOTATION

17. COSATI CODES			18. SUBJECT TERMS (Continue on reverse if necessary and identify by block number)
FIELD	GROUP	SUB-GROUP	Optical Processing, Lithium Niobate, Pattern Recognition, Barium Titanate, Associative Memory, Phase Conjugation
09	05		
12	09		

19. ABSTRACT (Continue on reverse if necessary and identify by block number)

Thesis Advisor: Steven K. Rogers, Maj, USAF
Associate Professor
Department of Electrical Engineering

20. DISTRIBUTION / AVAILABILITY OF ABSTRACT	21. ABSTRACT SECURITY CLASSIFICATION
☒ UNCLASSIFIED/UNLIMITED ☐ SAME AS RPT. ☐ DTIC USERS	UNCLASSIFIED
22a. NAME OF RESPONSIBLE INDIVIDUAL Steven K. Rogers, Assoc. Professor	22b. TELEPHONE (Include Area Code) (513) 255-9266 22c. OFFICE SYMBOL AFIT/ENG

DD Form 1473, JUN 86 — Previous editions are obsolete.

SECURITY CLASSIFICATION OF THIS PAGE
UNCLASSIFIED

This thesis investigates an all optical holographic associative memory (HAM) which uses iron doped lithium niobate as the holographic storage medium. Theoretical development of holographic recording and reading in thick, photorefractive material is performed. Initial experiments identify recording parameters which optimize the holographic diffraction efficiency of stored holograms. Increasing diffraction efficiency is reported during object beam illumination of the hologram. This unexpected result is linked to the use of a thin, anisotropic, plastic diffuser in the object beam.

The operational theory of a single iteration, multiple object HAM system is developed. Experiments are performed with the HAM, using a single stored object, to verify system operation. Distortion experiments are accomplished to qualitatively determine system performance when presented with a partial input. Complete object reconstruction was not achieved due to the single iteration HAM architecture. Experiments demonstrating holographic storage of multiple objects in Fe:LiNbO, using angle multiplexing were performed. The HAM system achieved reconstruction of any one of the stored objects. However, once a single object was reconstructed, subsequent memory recall of other stored objects failed due to the dynamic holographic medium. The generation of one output image distorted the remaining holograms such that additional reconstructions were not possible.

Lastly, a full resonant HAM operating in a closed loop optical cavity was investigated. Two phase conjugate mirrors were used to provide the feedback necessary for closed loop oscillations. However, current experimental constraints resulted in cavity losses that weakened the signal below the minimum threshold required for resonance. Suggestions for providing gain within the cavity and first order approximations of the required gain were provided.

AFIT/GEO/ENG/89D-3

NEURAL NETWORK ASSOCIATIVE MEMORY USING NON-LINEAR HOLOGRAPHIC STORAGE MEDIA

THESIS

Dwayne William Frye
Captain, USAF

AFIT/GEO/ENG/89D-3

Acknowledgments

I have received an enormous amount of help and support while working on this thesis. I would like to sincerely thank my advisor, Dr. Steven K. Rogers, for his patience and excellent guidance with regard to this research. In addition, I also thank the members of my thesis committee, Dr. Matthew Kabrisky and Dr. Theodore Luke, for their keen insight and helpful suggestions. Most importantly, I thank my wife Lisa for her patience, understanding, and support during this entire master's program, and in particular during the thesis research period.

I would like to dedicate this thesis research to the man who has always triggered my interest in science and engineering. He motivated my desire to learn, and for that I'm very grateful. Thank you, Dad. This one's for you.

Dwayne William Frye

Table of Contents

List of Figures

Abstract

This thesis investigates an all optical holographic associative memory (HAM) which uses iron doped lithium niobate as the holographic storage medium. Theoretical development of holographic recording and reading in thick, photorefractive material is performed. Initial experiments identify recording parameters which optimize the holographic diffraction efficiency of stored holograms. Increasing diffraction efficiency is reported during object beam illumination of the hologram. This unexpected result is linked to the use of a thin, anisotropic, plastic diffuser in the object beam.

The operational theory of a single iteration, multiple object HAM system is developed. Experiments are performed with the HAM, using a single stored object, to verify system operation. Distortion experiments are accomplished to qualitatively determine system performance when presented with a partial input. *Complete* object reconstruction was not achieved due to the single iteration HAM architecture. Experiments demonstrating holographic storage of multiple objects in $Fe{:}LiNbO_3$ using angle multiplexing were performed. The HAM system achieved reconstruction of any *one* of the stored objects. However, once a single object was reconstructed, subsequent memory recall of other stored objects failed due to the *dynamic* holographic medium. The generation of one output image distorted the remaining holograms such that additional reconstructions were not possible.

Lastly, a full resonant HAM operating in a closed loop optical cavity was investigated. Two phase conjugate mirrors were used to provide the feedback necessary for closed loop oscillations. However, current experimental constraints resulted in cavity losses that weakened the signal below the minimum threshold required for resonance. Suggestions for providing gain within the cavity and first order approximations of the required gain were provided.

NEURAL NETWORK ASSOCIATIVE MEMORY USING NON-LINEAR HOLOGRAPHIC STORAGE MEDIA

I. Introduction

The Air Force mission requires the capability to quickly identify and recognize objects. Presently, optical systems on board aircraft support pilots in performing these tasks. However, the pilot must still devote precious time and attention to the final recognition of identified targets. Automatic pattern recognition systems which locate and identify objects in real time would greatly reduce pilot workload during combat. Also, 'fire and forget' smart weapons which seek specific targets require the development of such autonomous recognition systems. Automatic pattern recognition can also be used to support general purpose robotics. Thus, the potential widespread utility of an autonomous pattern recognition system makes it of primary importance to the Air Force (20:1)(21:34).

Associative memories, defined as fault tolerant, content addressable memory systems, can recall complete noise free objects when addressed by partial or distorted input objects (22:1900). In an optical associative memory, objects of interest are holographically stored in a light sensitive medium, such as photographic film. When the memory system is addressed by a distorted version (input) of one of these stored objects, the system compares this input with all the stored objects. The system associates the input with that stored object which most closely resembles the distorted input. The associative memory system then generates, as the output, a complete, undistorted version of that particular stored object. A clear, complete

representation of the object can be generated from the (original) distorted input (9:2). Clearly, associative memories may be used as pattern recognition devices.

In addition, Dunning suggests that the fault tolerant associative properties of the holographic associative memory (HAM) system may be a paradigm for the way the brain processes information (22:1900). A large body of research in the area of neural network modeling has shown that associative memories are a key element in an all optical neural network computer (7:205). Therefore, the associative memory may also play a vital role in 'smart' computers which, like the human brain, learn from past mistakes and make appropriate corrections. The advantages of high speed performance that optical parallel processing can provide make the associative memory appealing for neural network computing as well as for real time pattern recognition.

This research is part of the Air Force's ongoing investigation into the holographic associative memory as an optical pattern recognition device and as the memory element of a neural network computer (9:1). In order to support the Air Force's need for autonomous pattern recognition and 'smart' computers, further research must identify and implement real time holographic storage media.

1.1 Problem Statement

This thesis research investigates the feasibility of using real time holographic material as the storage medium in an all optical holographic associative memory. The investigation provides a means for automatic pattern recognition and provides the memory required for an optical neural network computer.

The associative memory system uses a self pumped barium titanate ($BaTiO_3$) photorefractive crystal to provide phase conjugation for optically correlating the memory with the input object(s). This self pumped, phase conjugate architecture was originally developed by Dunning et al. (7:205). Another photorefractive material, iron doped lithium niobate ($Fe:LiNbO_3$) is used as the near real time holographic

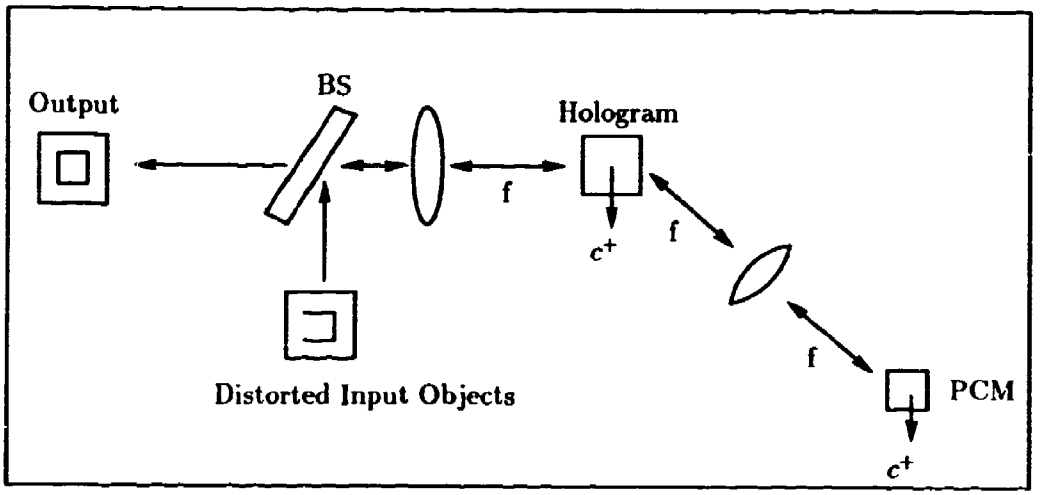

Figure 1. Single Iteration Holographic Associative Memory

storage media. This nonlinear crystal replaces the photographic plates used by Capt Fielding during his AFIT thesis research (10:851). The architecture for the single iteration holographic associative memory used in this research is shown in Figure 1.

1.2 Summary of Current Knowledge

Recent versions of the holographic associative memory (HAM) have been implemented by Fielding; Owechko, Dunning, Marom, and Soffer; Anderson, White, Aldridge, and Lindsay; and Yariv and Kwong (9:2). The memory storage capacity and achievable signal to noise ratio (SNR) of these versions of the HAM were limited because of cross–talk between the stored objects. This cross–talk degrades the ability of the system to generate a complete, undistorted object from a distorted input.

Dunning and Owechko have implemented an all optical holographic associative memory using phase conjugate mirrors (photorefractive crystals) to support correlation of the distorted input with the objects stored in non–real time holographic memory (22:1902). These photorefractive crystals provide gain to the system and

also reduce the cross-talk between stored objects. According to Dunning, the reduction of cross-talk has greatly increased the storage capacity of the HAM (22:1900). Experimental results demonstrate that the memory can recall complete, undistorted objects when presented with as little as twenty percent of one of the stored objects (6:348).

Capt Fielding studied the use of photographic film plates as the storage medium for the holographic memory (9:31). Chemical development of these plates required the removal of the hologram from the optical system and subsequent realignment during object recall. Capt Fielding states, "The hologram had to be replaced within 15 micrometers of its original position to satisfy the requirements of object reconstruction. Replacing the hologram exactly was a tedious process which could take up to ten minutes" (9:42). Obviously, a system which incorporates photographic plates as the storage medium presents unsolvable hurdles for real time pattern recognition. However, as Dunning et al. point out, replacing the holographic recording medium with real-time media (such as photorefractive crystals) would make real-time modification of the hologram possible (7:210).

The storage of holographic images in photorefractive materials has been investigated since the early 1960's. Weaver and Gaylord indicate that non-linear crystals are capable of storing large quantities of data. "Through optically induced refractive index changes (electro-optic effect), very thick, phase holograms may be recorded in photorefractive crystals such as lithium niobate" (30:404). Presently, up to 500 holograms have been recorded in a single lithium niobate crystal (8:169).

In 1972, Phillips et al. published a detailed study of the optical and holographic storage properties of metal doped lithium niobate. That study found the optical storage of information in lithium niobate ($LiNbO_3$) to rely on the presence of localized centers in the material containing electrons that could be optically excited into the electronic conduction band. These electrons diffuse within the material until they become trapped at local impurity sites in the material. This 'shuffling' of

electrons creates an electric field distribution within the material which modulates the material's refractive indices via the electro-optic effect. The result is that light entering the crystal will be transmitted at different angles, depending on where the light is incident on the crystal. This modulation of refractive index, often referred to as a 'grating,' forces the light transmitted through the crystal to travel in a specific direction (23:95). This is exactly the same effect a hologram stored in the crystal will have on transmitted light. Phillips et al. found that the introduction of impurity metals (such as iron, copper, and nickel) increased the optical sensitivity of the material and hence enhanced the generation of the grating (23:101). The research clearly identified iron as the best dopant material. Iron doped $LiNbO_3$ crystals were found to have a 500 fold increase in optical sensitivity over undoped $LiNbO_3$. The diffraction efficiency was experimentally found to approach 100 percent for iron doped $LiNbO_3$ (23:108).

More recently, Weaver has reported two limiting effects on diffraction efficiencies in volume holograms in lithium niobate. "One effect is the limit due to scatter noise that determines the minimum value of diffraction efficiency. The second effect is a shift in the Bragg angle" (29:110). The scatter noise results from the light incident on the crystal scattering off the holographic grating in undesired directions. The Bragg angle is defined as the angle between the surface normal of the crystal and the direction in which the incident light beam approaches the crystal. Any deviation in this angle during illumination of the hologram will decrease the holographic diffraction efficiency.

The many journal articles and research reports describing holographic storage in photorefractive crystals (such as lithium niobate) establish that this process is well understood. However, little has been published regarding the use of these materials as the holographic storage medium in associative memories. Most recently, Psaltis et al. published an article describing the use of photorefractive crystals as the storage media in adaptive optical neural networks (24:1752). Specifically, the advantage of

dynamic modification of the holographic memory and the maximum storage capacity of a photorefractive volume hologram are investigated. "Photorefractive crystals are particularly attractive as holographic media in this application (neural computers) because it is possible to record information in these crystals in real time at very high densities without degrading the photorefractive sensitivity" (24:1754). As is evident from this recent article, the use of photorefractive crystals as the storage medium in associative memory systems for use in optical pattern recognition and neural network computing is a valid and important area of research.

1.3 Scope

This research demonstrates the feasibility of using photorefractive materials as the storage media in holographic associative memories. As this is a proof of concept experiment, no attempt is made to optimize the material selected as the holographic storage medium. Lithium niobate has been selected as the storage material because it is well understood and widely used in holography. While $LiNbO_3$ is not classified as a real time material due to its response time to optical energy (typically seconds), it nevertheless clearly demonstrates the usefulness of photorefractive materials in associative memory systems.

Initial experiments will be performed to identify the critical recording parameters affecting the diffraction efficiency of holograms stored in iron doped lithium niobate. Examples of parameters of interest are the reference to object beam power ratio, total power incident on the crystal, angular separation between the reference and object beams, crystal orientation, and beam polarization.

Experiments using the Holographic Associative Memory shown in Figure 2 will be performed. The general architecture (optical layout) for the research will be the same as that used by Fielding (9:3). This holographic associative memory, which employs phase conjugation, is based on the Hughes Research Corporation's holographic associative memory (9:4). The system's ability to function while using

a non–linear holographic medium will first be demonstrated. The capability of the system to recall *complete* output objects from distorted inputs will then be investigated. Finally, the performance of this HAM architecture during multiple object storage and subsequent memory recall will be determined.

In an effort to support ongoing Air Force investigations by the Rome Air Development Center's Photonics Laboratory (concerning the usefulness of this basic HAM architecture in optical neural network computing), experiments with a full resonant HAM system operating in a closed loop optical cavity will be performed.

The main goal of this research is to perform a detailed evaluation of the capabilities and limitations of both the single iteration and closed loop HAM systems. As a result, the effectiveness of these systems for solving Air Force requirements in autonomous pattern recognition and optical computing can be estimated.

1.4 Approach

This research will be accomplished in four main parts. First, an investigation of the principle components of the holographic associative memory, with particular emphasis on the holographic storage medium, will be performed. Theoretical development and experimental techniques for recording and reading holograms using $LiNbO_3$ will be evaluated. Specific areas to be considered are exposure time, beam energies, beam polarizations, crystal orientation, and angular selectivity of the crystal. A theoretical understanding of the phase conjugation properties of $BaTiO_3$ will be developed and the experimental results of Capt Fielding's work using $BaTiO_3$ shall be reviewed. This research effort uses the same $BaTiO_3$ crystal (for phase conjugation) that Capt Fielding characterized, therefore the experimental measurements Fielding made are assumed to remain valid (9:19).

Once the holographic and phase conjugation concepts are well understood, the second thrust of the research begins. Specifically, the $LiNbO_3$ crystal will be implemented in the associative memory architecture. The correct alignment of optical

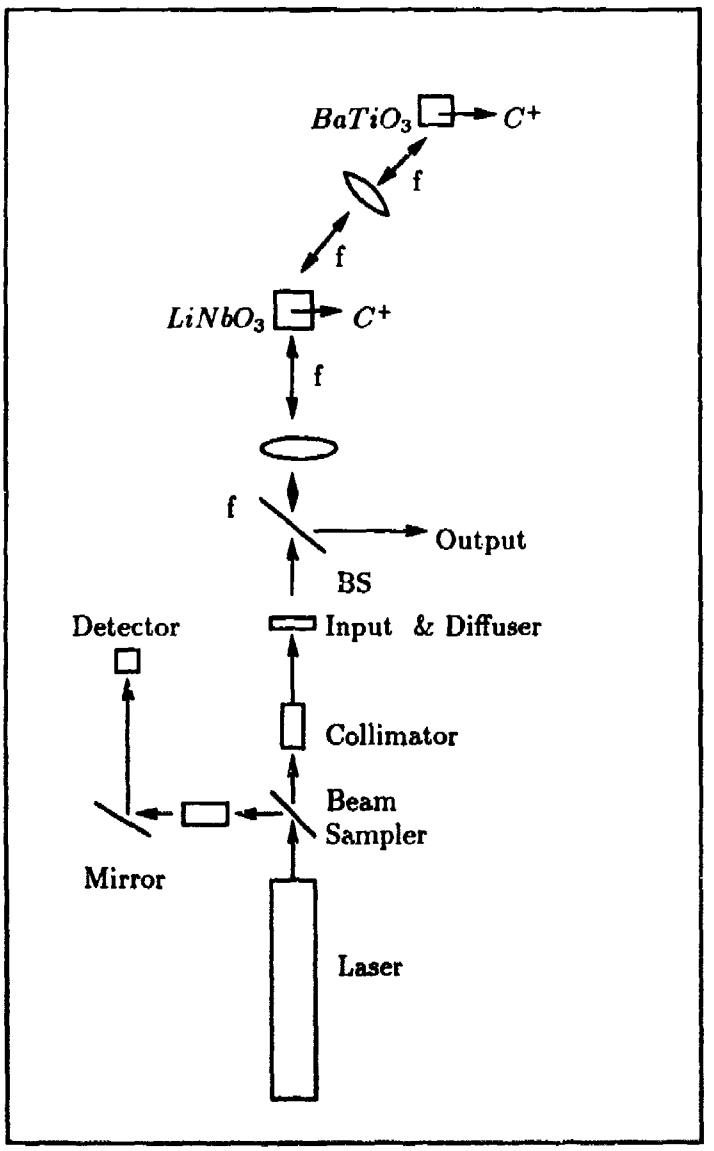

Figure 2. The Holographic Associative Memory

components will be verified by storing a simple object in the memory and allowing the associative memory to reconstruct the object from a slightly distorted input. The physical limitations of the system, such as maximum allowable input object distortion, will be investigated.

Part three of the research will demonstrate the capability of the memory to perform multiple object recall through the use of angular multiplexed holographic storage. Several different objects will be stored, using various reference beam angles, and the response of the system to distorted inputs will be observed.

The final part of the research considers a full resonant, multiple iteration Holographic Associative Memory. Experiments with a system that uses two $BaTiO_3$ crystals to form a closed loop, resonant cavity are carried out to investigate the physical limitations on performance.

The following chapter investigates the implementation of photorefractive materials as the holographic storage medium for an associative memory. Specifically, the advantages, theoretical development, and experimental results of using photorefractive holographic media are discussed. Chapter Three develops the theory and optical architecture for a single iteration holographic associative memory. Chapter Four describes the actual development and testing of a holographic associative memory which uses an iron doped lithium niobate crystal as the holographic storage medium. The procedures followed in testing the system and experimental results obtained are identified and discussed. The Fifth Chapter investigates a fully resonant HAM system implemented to enhance complete pattern reconstruction from distorted, incomplete input objects. The final chapter summarizes the key results of this research effort and identifies areas where further research may prove fruitful in supporting possible applications of such a 'real time' holographic associative memory.

II. Real Time Holographic Storage

2.1 Introduction

As indicated in the previous chapter, a key component of the holographic associative memory is the hologram. The hologram serves as the memory unit of the system, storing information for subsequent recall. In addition, the hologram is a vital component in an optical neural network. In this case, the hologram acts as a set of weighted interconnections between neurons which comprise the network (24:1752).

Regardless of the application, the need for real time operation of the holographic associative memory remains. Autonomous system operation requires dynamic, real time holographic media which can record, store, and read information in very short periods of time. This chapter discusses the advantages, theoretical development, and experimental results of using photorefractive (non-linear) crystals as holographic storage media.

2.2 Advantages Of Dynamic Photorefractive Holographic Storage Media

One class of materials which are ideally suited for holographic applications are photorefractive crystals. These materials possess properties which satisfy the demanding requirements imposed upon dynamic holographic media. "These properties include instantaneous hologram formation (self-development), high data storage capacity via volume superposition, high sensitivity and resolution, erasability and reusability, fast recording and readout, and hologram fixing" (19:81).

In contrast to photographic plates, which (after exposure) must be removed, chemically developed, and carefully re-inserted, photorefractive materials respond to exposure in such a manner as to 'immediately' form a holographic grating. Thus, the problems of chemical development are eliminated, and the speed of holographic

formation is dramatically improved. The theoretical details of holographic formation in photorefractive crystals will be discussed in the next section.

In addition, as Eichler et al. point out, volume superposition provides high data storage capacity.

> A very attractive feature of a holographic system is the possibility of volume storage. In a photosensitive medium where bulk changes are produced, many holograms can be superimposed in the same element of volume. A single hologram of about 1 mm^2 area may contain 10^4 bits or more. Presently up to 500 holograms can be superimposed reversibly at each site in $LiNbO_3$ crystals, giving a total capacity of 0.5 Gbits per cm^2 (8:169).

This multiple storage is achieved by varying the angle of incidence of the reference beam (angle multiplexing) for each individual hologram. The limitation on storage capacity is therefore partially determined by the minimum deviation of the reference beam which allows resolvable holographic formation. Weaver has indicated that holograms stored in $Fe:LiNbO_3$ may be angularly multiplexed with a minimum angle separation equal to the half-power, full width divergence of a corresponding plane wave hologram (30:410).

Optical photosensitivity may be defined as "the incident optical energy required for a given diffraction efficiency and hologram thickness. Ultimate recording sensitivity comparable to ones obtained in high resolution photographic plates . . . can be obtained" (8:163). In the case of iron doped $LiNbO_3$, the sensitivity has been found by Phillips et al. to depend approximately linearly on the Fe^{2+} absorption at 4880 angstroms. As stated in Chapter One, iron doped lithium niobate has shown a 500 fold increase in optical sensitivity over undoped $LiNbO_3$ (23:95). In addition to high sensitivity, $LiNbO_3$ also has excellent resolving capabilities. Chen et al. have reported poled, single domain crystals of $LiNbO_3$ with resolution in excess of 1600 lines per millimeter (4:223).

Another useful property of photorefractive crystals is that holograms can either be permanently stored or continuously erased. Permanent storage would be very beneficial in 'read only' type applications, where the stored information must remain intact. Erasable holograms would allow dynamic modification of the stored information for applications such as implementing learning algorithms in an optical neural network. In lithium niobate, permanent storage is achieved by thermally cycling the crystal containing the holographic grating (3:86). Erasure is achieved by homogeneous illumination of the crystal (8:163).

In order for photorefractive crystals to satisfy the requirements for real time holographic media, they must be able to record, store, and read out information very quickly. Eichler et al. report that short writing and erasure times can be achieved through the use of pulsed lasers with high energies. "Experiments with frequency doubled Nd:Yag lasers at 530 nanometers showed optical writing, reading, and erasure of refractive index gratings are possible on a nanosecond time scale or even faster" (8:71). Shah reports holographic recording, storage, and retrieval in 30 nanoseconds in $LiNbO_3$ using pulsed lasers (25:131). These short times indicate photorefractive crystals can indeed provide real time holography.

2.3 Theoretical Development Of Holographic Storage In Photorefractive Crystals

In order to fully understand the process of holographic recording, storage, and read out of information in photorefractive crystals, the basic characteristics of these materials should be discussed.

The optical properties of these materials depend on the direction of propagation as well as the polarization of the light waves incident on the material (33:69). For example, a plane wave normally incident upon an anisotropic crystal will generate two independent solutions to Maxwell's wave equation for propagation within the material. Each wave will travel with a unique phase velocity, and the two waves will be linearly polarized, perpendicular to one another. The two independent polar-

ization directions play a critical role in reading the grating formed by the modulation of the material's index of refraction. In addition, correct selection of one of these polarization directions for the input beam during reading can significantly increase the diffraction efficiency of a hologram stored in anisotropic material. The theoretical explanation for this 'polarization sensitivity' is given below.

Anisotropic crystalline materials may be further subdivided, based upon the inherent symmetry of the crystals. Specifically, the physical properties are influenced by the point group symmetry elements of the crystal (32:54). Cubic crystals, for example, are always isotropic. Anisotropic materials are either uniaxial or biaxial, which indicates whether the material contains one or two *optic axes*. The optic axes are defined as those directions within the material along which both independent wave solutions travel at the same velocity (32:81). $LiNbO_3$ is an example of an uniaxial crystal with a trigonal point group symmetry (3–fold axis of symmetry)(32:55).

Light travelling in $LiNbO_3$, in any direction other than along the optic axis, will be broken into the two independent waves described above. Each wave travels at a different phase velocity (with a unique Poynting vector direction), thus there are

> two velocity surfaces. One is spherical, ... and is the ray–velocity surface of the *ordinary ray*. The other is an ellipsoid of revolution and is the ray–velocity surface of the *extraordinary ray* (32:81).

These two surfaces, which represent non–trivial solutions to the Fresnel equation within the material, can be geometrically represented by a three dimensional 'wave normal' surface (33:72). Figure 3 shows the intersection of the normal surface with the xz plane for a negative uniaxial crystal, such as lithium niobate (33:84).

The formation of a hologram in a photorefractive crystal relies on the modulation of the refractive indices within the material. Chen et al. originally demonstrated the formation of pure phase, volume holograms in $LiNbO_3$ (4:223). The mechanism

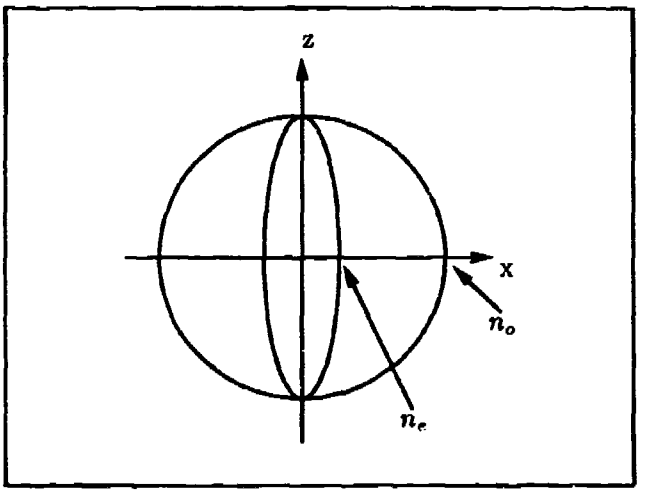

Figure 3. Wave Normal Surface in XZ Plane of Negative Uniaxial Material

by which the hologram is formed has been described by Amodei and Staebler as follows:

> Exposure of such a medium to the light-interference pattern constituting the hologram excites electrons from the [impurity] traps to the conduction band at rates that are proportional to the light intensity at any given point. This gives rise to an inhomogeneous concentration of free carriers that diffuse thermally, or drift under applied or internal electric fields, and become re-trapped preferentially in regions of low-intensity light. The net result is a net space-charge pattern that is positive in regions of high intensity and negative in regions of low intensity. The space charge generates a field that modulates the index of refraction via the electro-optic effect and gives rise to a phase hologram (3:75).

It is known that the application of either an internal or external field to certain anisotropic crystals creates a change in both the dimensions and orientation of the index ellipsoid. This effect is referred to as the *electro-optic effect*. "The electro-optic effect affords a convenient and widely used means of controlling the phase or intensity of optical radiation" (33:220).

The following development follows closely that of Yariv and Yeh (33:223). The index ellipsoid assumes its simplest form in the principal coordinate system:

$$\frac{x^2}{n_x^2} + \frac{y^2}{n_y^2} + \frac{z^2}{n_z^2} = 1 \tag{1}$$

x, y, and z are the principal axes. The principal axes are defined as those directions which represent the eigendirections of the material's electro-optic tensor. n_x, n_y, and n_z represent the three principal indices of refraction within the material. For a uniaxial crystal, $n_x = n_y \neq n_z$. The ordinary and extraordinary indices of refraction are defined, by convention, as follows:

$$n_o = n_x = n_y$$

$$n_e = n_z$$

In the presence of an electric field, the equation of the index ellipsoid can be written

$$\left(\frac{1}{n_x^2} + r_{1k}E_k\right)x^2 + \left(\frac{1}{n_y^2} + r_{2k}E_k\right)y^2 + \left(\frac{1}{n_z^2} + r_{3k}E_k\right)z^2 + 2yzr_{4k}E_k + 2zxr_{5k}E_k + 2xyr_{6k}E_k = 1 \tag{2}$$

where the r_{ik}'s represent the electro-optic coefficients and the E_k's (k = 1,2,3) represent the applied field components, with summation assumed over the principal coordinates. Equation 2 reduces to Equation 1 when no applied field is present.

For an electric field applied along the optic axis of $LiNbO_3$, Equation 2 reduces to the following:

$$\left(\frac{1}{n_o^2} + r_{13}E\right)x^2 + \left(\frac{1}{n_o^2} + r_{13}E\right)y^2 + \left(\frac{1}{n_e^2} + r_{33}E\right)z^2 = 1 \tag{3}$$

Since no mixed terms appear in Equation 3, the principal axes of $LiNbO_3$ are

not rotated as a result of the applied field. The crystal remains uniaxial, with the lengths of the new semiaxes of the ellipsoid given by

$$n_x = n_y = n_o - \frac{1}{2} n_o^3 r_{13} E \tag{4}$$

$$n_z = n_e - \frac{1}{2} n_e^3 r_{33} E \tag{5}$$

From the above equations, one can see that for maximum refractive index modulation (and hence large diffraction efficiency), the orientation of the crystal during recording is critical. The maximum refractive index modulation occurs for the special case when the optic axis is perpendicular to the bisector of the two interfering waves. This orientation results in a generated internal field along the c axis of the crystal, therefore maximizing E in the above equations. For maximum diffraction efficiency during read out of the hologram, the polarization of the read beam should be in the plane formed by the optic axis and this bisector (extraordinary polarization) (3:81). In this case, the birefringence for a wave propagating along the x direction is given by

$$n_z - n_y = (n_e - n_o) - \frac{1}{2} \left(n_e^3 r_{33} - n_o^3 r_{13} \right) E \tag{6}$$

For $LiNbO_3$, the values of these constants at 4880 angstroms are $n_o = 2.37$, $n_e = 2.27$, $r_{13} = 8.6$, and $r_{33} = 30.8$. The electro–optic coefficients are in units of 10^{-10} cm per volt.

The following theoretical development of holographic formation in $LiNbO_3$ follows closely that of Eichler et al. (8:161) and that of Collier et al. (5:10). The light–interference pattern required to form a hologram in $LiNbO_3$ is generated by the interference of two coherent wavefronts. These wavefronts are labeled E_o and E_r, for object and reference, in Figure 4. The object wavefront contains the object phase and amplitude information to be stored in the hologram. For this research

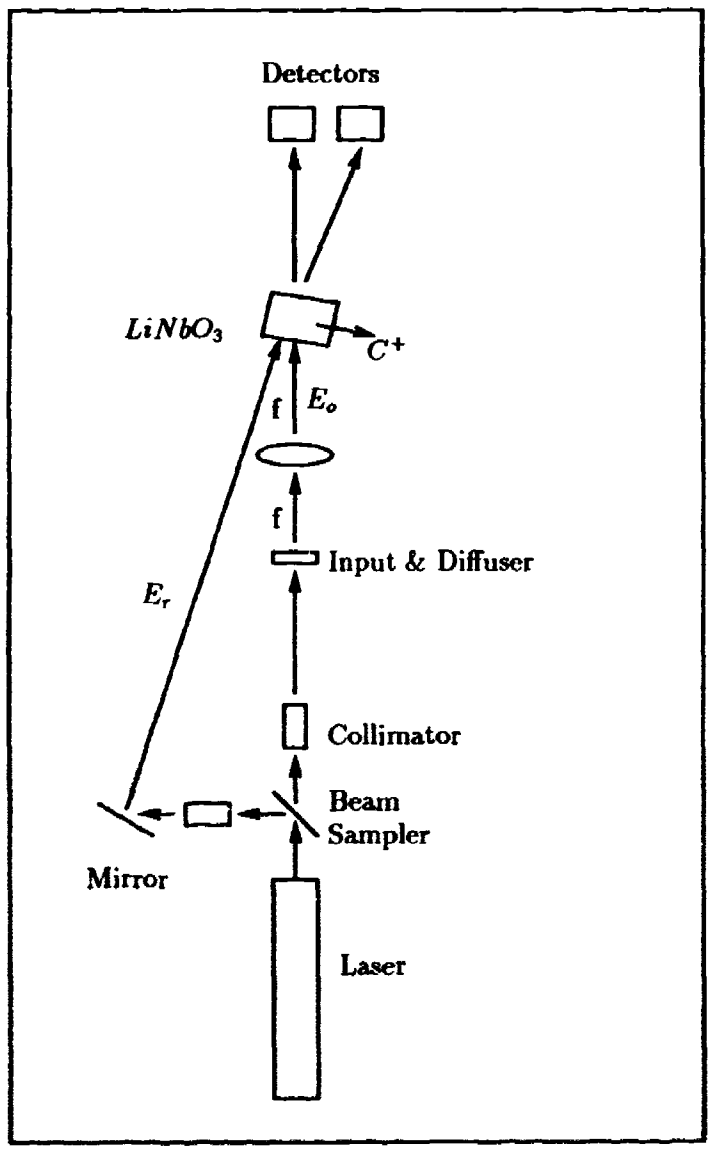

Figure 4. Holographic Recording in $LiNbO_3$

effort, only two dimensional transparent objects were considered.

The equations describing these two wavefronts are listed below:

$$E_o(f_x, f_y) = E_o(f_x, f_y)\cos(\omega t - \varphi_o) = Re\left\{A_o(f_x, f_y)\exp^{i\omega t}\right\} \tag{7}$$

and

$$E_r(f_x, f_y) = E_r(f_x, f_y)\cos(\omega t - \varphi_r) = Re\left\{A_r(f_x, f_y)\exp^{i\omega t}\right\} \tag{8}$$

The interference pattern is simply the sum of these complex fields:

$$E(f_x, f_y) = E_o(f_x, f_y) + E_r(f_x, f_y) \tag{9}$$

The refractive index modulation in the crystal responds to the *intensity* variation of the total field within the crystal:

$$I(f_x, f_y) = |E(f_x, f_y)|^2 = (A_o + A_r)(A_o^* + A_r^*) \tag{10}$$

where the A_o^* denotes spatial complex conjugate. For a phase grating, the *phase shift* of the transmitted wave φ_t will be proportional to the intensity:

$$\varphi_t(f_x, f_y) = \gamma I(f_x, f_y) \tag{11}$$

This phase shift corresponds to a complex transmittance given below:

$$T_p(f_x, f_y) = \exp^{i\varphi_t(f_x, f_y)} = \exp^{i\gamma I(f_x, f_y)} \tag{12}$$

Assuming $\gamma I(f_x, f_y) \ll 1$ radian and $\exp^x = 1 + x + \frac{x^2}{2!} + \cdots$, then

$$T_p(f_x, f_y) = \exp^{i\gamma I(f_x, f_y)} \approx 1 + i\gamma I(f_x, f_y) \tag{13}$$

This complex transmittance represents, in the most general terms, the holo-

graphic grating formed in the photorefractive crystal. During the implementation of the real time associative holographic memory system, this hologram will be illuminated with a distorted version of the original stored object. The theoretical development of the equations describing the HAM's operation with a distorted input will be described in the following chapter. However, in order to understand the holographic 'reading' process, the equations describing the illumination of the hologram with the original reference beam follow:

$$A_t(f_x, f_y) = A_r(f_x, f_y)\, T_p(f_x, f_y) \tag{14}$$

$$= A_r(f_x, f_y)\,(1 + i\varphi_t(f_x, f_y)) \tag{15}$$

where $A_t(f_x, f_y)$ represents the transmitted waves out of the hologram. Substituting for $\varphi_t(f_x, f_y)$ and dropping the (f_x, f_y) notation

$$A_t = A_r + iA_r\gamma I \tag{16}$$

$$= A_r + iA_r\gamma\,(A_o + A_r)\,(A_o^* + A_r^*) \tag{17}$$

$$= A_r + i\gamma A_r|A_o|^2 + i\gamma A_r|A_r|^2 + i\gamma A_o|A_r|^2 + i\gamma A_r^2 A_o^* \tag{18}$$

The only term of interest in Equation 18 is the fourth term. This term represents the wavefront traveling in the original object beam direction. It is the recreation of the original object wavefront.

2.4 Experimental Development

This section describes the procedures used to experimentally determine the optimum configuration for recording holograms in iron doped $LiNbO_3$. 'Optimization', in this case, is based upon the holographic medium's ultimate purpose as the storage mechanism within the holographic associative memory. Specifically, high

resolution holographic images and a strong first order diffracted beam (when illuminating the hologram with the *object* beam) are desired, based upon the operational requirements of the HAM.

To obtain these desired characteristics, diffuse Fourier transform holograms were recorded. The Fourier transform of the object is recorded to allow access to the correlation domain during re-illumination by a partial or distorted input (9:2). The 'cross-correlation' of the distorted input with the objects stored in memory is a desired characteristic typical of Vander Lugt type filters commonly used in coherent processing (13:177). However, one drawback to using Fourier transform holograms is that

> light passing through the [object] transparency undeviated (zero-order) is focused by the lens to a high-intensity peak at the origin of the frequency or hologram plane. By comparison, the higher spatial frequencies diffracted by the transparency and focused to other regions of the frequency plane are much less intense (5:209).

As a result, the relative diffraction efficiency may be poor for these high frequency components.

A phase diffuser placed in the object beam path alleviates this unwanted effect. The transmitted light from the object-diffuser combination scatters from each point on the object across the entire holographic medium. There is therefore no longer a one to one correspondence between a portion of the hologram and a point on the object. Thus, the array of 'bright spikes' resulting from the object's Fourier transform are distributed evenly over the recording plane (26:9). In addition,

> this property of the diffuse light hologram to record information in a non-localized way makes it attractive for information storage. In contrast to storing information by means of micro-images where a scratch or blemish entirely removes or obliterates information, information stored

in a hologram made with diffuse subject light is relatively immune to such imperfections of the recording medium (5:197).

The diffuser used for this research was a thin sheet of plastic taped directly onto the object transparency (reference Figure 4).

It should be pointed out that one of the common benefits of using Fourier transform holography does not apply to this research. For *thin* holographic media, use of Fourier transforms allows image reconstruction in the presence of slight holographic translation (5:209). However, the use of thick, volume holograms eliminates the shift invariance of the correlation between the input and stored objects (24:1754). The loss of shift invariance is due to the Bragg angle selectivity requirements imposed by the grating in a thick medium (5:14). Angular selectivity describes the need for the reference beam to illuminate the hologram at a precise angle in order to achieve reconstruction (11:4771). "Maximum diffraction occurs when the grazing angles of incidence and reflection are equal" (5:14). The Bragg condition is often given by the following equation:

$$n\lambda = 2d\sin\theta \tag{19}$$

θ is both the angle of incidence and reflection from the grating, d is the thickness of the medium, and n is any positive integer (32:20). In non-linear optic applications, the Bragg angle requirement is often referred to as the 'phase match' condition (8:36). For thick gratings, the input beam is diffracted by each grating element and becomes advanced in phase. The parameter Q is used to quantify this phase shift:

$$Q = \frac{2\pi d\lambda}{\Lambda^2 n} \tag{20}$$

where d = hologram thickness, Λ = grating spacing, and n is the index of refraction in the medium. For phase differences sufficiently small ($Q \ll 1$), the diffracted beams constructively interfere. However, if $Q \gg 1$, only one diffracted wave is observed (8:100). For the optical architecture used in this research, Q is equal to a phase

shift of 90 degrees (14:226). Thus, only one diffracted wave should be observed. Experimental results support this conclusion.

The holographic storage medium used in this research was a 10 x 10 x 10 mm^3, 0.015 percent iron doped, electrically poled, single domain $LiNbO_3$ crystal. Only the y faces of the crystal were polished. The optical configuration for recording is shown in Figure 4. A Spectra Physics Model 2020–3 argon ion laser, operating in a single longitudinal mode at 4880 angstroms (with internal étalon), provided the linearly polarized coherent reference and object beams. The reference beam diameter was approximately 6 mm. All beam diameters were kept within the active area of the detectors, thus power (and not irradiance) was measured and recorded.

The first experiment was performed to identify the positive c–axis direction of the crystal. The procedure implemented relied on the fact that during two wave mixing, energy is transferred in the direction of the positive c–axis after the beams transverse the crystal (16:3). A reference beam of 4.1 mW and an object beam of 20.9 mW were allowed to couple within the crystal and the powers of each transmitted beam beyond the crystal detected and plotted. Energy transfer was readily observed. To ensure correct determination of the positive c–axis, the crystal was rotated 180 degrees and the experiment repeated. Energy was now transferred to the other beam, as expected. During both experiments, the normal to the positive c–axis bisected the angle between the reference and object waves. The polarization of both beams was in the plane formed by the bisector and the c–axis (extraordinary).

Once the c–axis direction was determined, the crystal was orientated such that energy would always be coupled towards the diffracted beam when illuminated by the *object* beam. This orientation was maintained for the remainder of the research because it serves to amplify the beam entering the phase conjugate mirror in the holographic associative memory system. Figure 4 shows the positive c–axis direction for the $LiNbO_3$ crystal.

The following three paragraphs describe the experimental procedures used to

identify optimum recording parameters for maximizing the holographic diffraction efficiency. The diffraction efficiency was calculated by dividing the power diffracted into the original reference beam direction by the power of the incident object beam. Fresnel surface losses were not considered because typical operational systems would encounter these same losses. The plots that follow identify diffraction efficiency (as a percentage) versus the parameter under investigation. Interpretation of the experimental results is discussed in the next section.

The next step in the hologram experiments was to determine the reference to object beam power ratio which would provide maximum diffraction efficiency. The object, stored during 60 second exposures, was a standard Air Force resolution chart with a plastic diffuser attached. The diffraction efficiency was measured by blocking the reference beam and measuring the percentage of light diffracted in the reference beam direction when the hologram was illuminated by the object beam. Fresnel face reflections (off of the $LiNbO_3$ crystal) were not considered in the diffraction efficiency measurements. The total power incident on the crystal was maintained between 15 and 25 mW for this experiment. Figure 5 is a plot of the diffraction efficiency versus time for varying reference to object beam ratios.

Once the optimum ratio was identified, the effects of changes in total power incident on the crystal were investigated. The reference to object beam ratio was set at approximately five to one, and the output power of the laser source incrementally increased. Figure 6 shows a plot of the diffraction efficiency versus time for several different values of total power incident on the crystal.

The last holographic experiment considered effects of object beam polarization during recording and reading. The plastic diffuser implemented was anisotropic. Thus, rotating the plastic relative to the object beam caused the object beam polarization to also rotate. The effects on holographic formation and diffraction efficiency due to object beam polarization were investigated by incrementally rotating the phase diffuser. The reference to object beam power ratio and the total power inci-

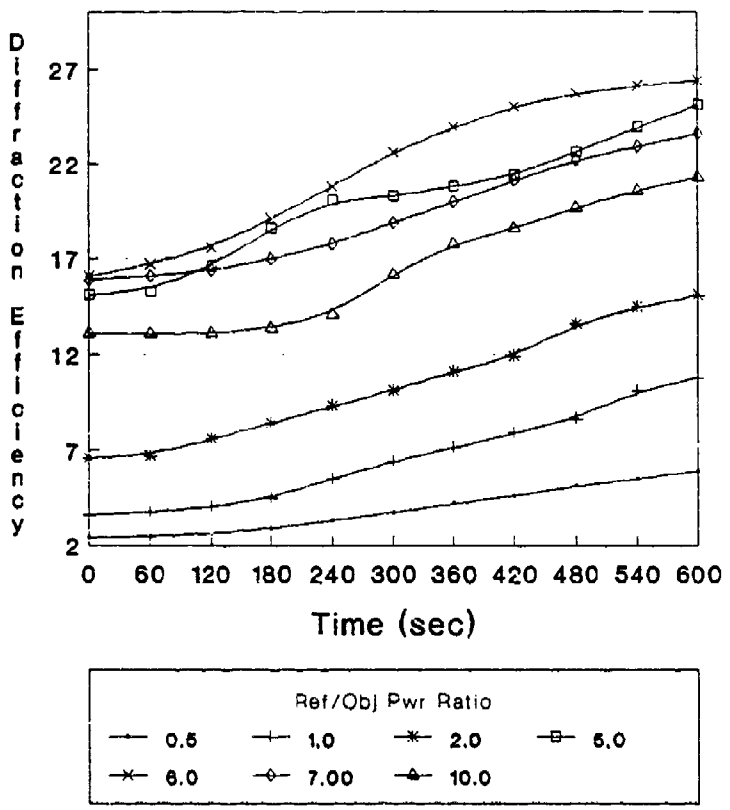

Figure 5. Reference to Object Beam Power Ratio Effects on Diffraction Efficiency

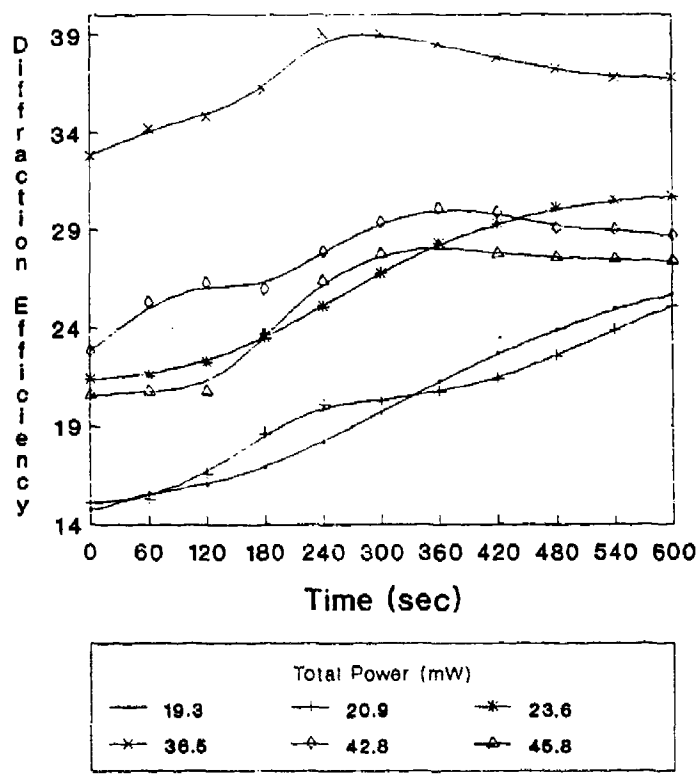

Figure 6. Total Incident Power Effects on Diffraction Efficiency

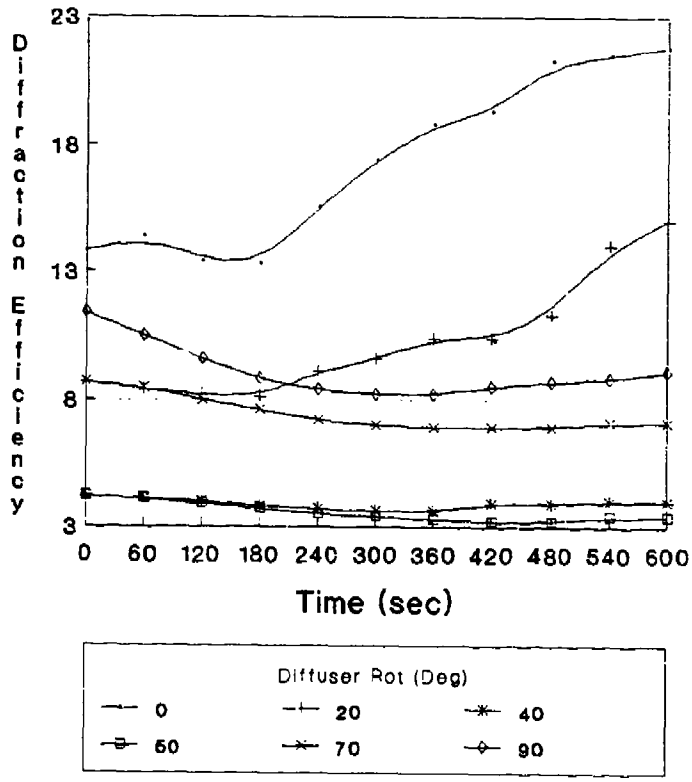

Figure 7. Read Beam Polarization Effects on Diffraction Efficiency

dent on the crystal were held constant. The phase diffuser was spatially separated from the object transparency for this experiment so that the diffuser could be rotated independent of the object. Thus, the results would not be impacted by rotations of the object. The diffuser was initially aligned so as to not rotate the object beam polarization, and a hologram was recorded and read. This process was repeated, while rotating the polarizer ten degrees for each iteration. Figure 7 plots the diffraction efficiency versus time for several angles of diffuser rotation.

2.5 Analysis of Holographic Results

From Figure 5, one can see that the power diffracted into the reference beam direction *increased* with time. This result was unexpected. Increasing diffraction efficiencies are typical of 'thermally cycled' fixed holograms (3:87), but the holo-

grams used in this research were not thermally cycled. It should be emphasized that the holograms were read with the diffuse Fourier transform of the object, and not the reference beam. However, when the holograms were illuminated with the reference beam (to measure the reconstructed image quality), the diffraction efficiency decreased with time, as expected. To investigate the effects of the diffuser (which was aligned so as to not rotate the object beam polarization during these reference to object beam ratio experiments), a hologram was written without the diffuser. Upon reading the hologram with the object beam, the diffraction efficiency fell to the $\frac{1}{e}$ point in approximately 120 seconds. This response time is typical of iron doped lithium niobate (2:541). According to Staebler and Amodei, interference during readout influences the readout erase time, consistent with previously observed enhancement of fixed holograms. The interference during readout effectively generates a 'new' grating in the medium. "Thus, it is clear that this 'new' hologram can either enhance or diminish the over-all diffraction efficiency" (27:1045). The enhancement rate in their experiment was not large enough to actually increase the over-all diffraction efficiency, but it did increase the total time required to erase the hologram (27:1048). Apparently, the presence of the anisotropic diffuser in this research is strongly enhancing the diffraction efficiency measured.

Upon closer inspection of the anisotropic diffuser (a Newport Corporation optical lens shipping bag), striations running parallel to one of the polarization axes were observed. The polarization axes lie along the major dimensions of the bag; that is, from top to bottom and from side to side (0 degrees and 90 degrees in Figure 7). The striations effectively form a grating which creates a 'cigar shaped' light distribution pattern in the back focal plane (hologram plane). The pattern is similar to that of a diffuse diffraction pattern from a series of narrow slits. Rotating the diffuser, and therefore the striations, caused a subsequent rotation of the 'cigar shaped' light pattern. Thus, not only is the diffuser spreading the spatial frequency components of the object, but it is also superimposing on the object wave the optical effect of the

grating present in the plastic. This object wave–plastic grating combination appears to be enhancing the overall diffraction efficiency. In order to isolate and identify the specific cause of this effect, further experiments investigating the diffraction efficiency of holograms recorded and read with just the diffuser as the 'object' should be performed.

Figure 5 shows that for an Air Force resolution chart–diffuser object combination, a reference to object beam power ratio of approximately 6.0 to 1 provides the highest diffraction efficiency. The maximum efficiency obtained during the ten minute reading period was 26.4 percent.

From Figure 6, one can see that increasing the total power incident on the crystal served to increase the diffracted power during read out. As the total power was raised, the power in the read beam was raised proportionally, so one would expect the diffracted energy to increase. However, as the total incident power was increased beyond 37 mW, the diffraction efficiency began to decrease. It is believed that undesired scatter off of the grating diminished the energy diffracted in the reference beam direction. As Staebler et al. point out, recording more intense holograms results in optical scattering (28:182). The maximum diffraction efficiency (39 percent) was obtained with 36.5 mW of power incident on the crystal.

Lastly, the effects on hologram diffraction efficiency due to object beam polarization are shown in Figure 7. As expected, variations in polarization during recording had little effect. As Chen indicates, the polarization of the writing beam was not critical to holographic formation (4:223). However, as the figure indicates, deviations from extraordinary polarization during reading significantly reduced the energy in the diffracted wave during read out. The polarization is extraordinary when the diffuser is at 0 degrees rotation. The reduction in diffracted wave energy results from the excitation of the smaller r_{13} electro–optic coefficient as the polarization becomes ordinary during reading. In order to achieve maximum diffraction efficiency, the r_{33} electro–optic coefficient must be excited during reading. This is

achieved by ensuring the read beam (object beam) is polarized in the plane formed by the c-axis and the direction of beam propagation.

In addition, the data also shows the apparent effect of the inherent grating present in the diffuser. The angles selected for diffuser rotation (to vary the polarization) were specifically chosen to be symmetric about the bisector between the two polarization directions within the diffuser. Thus, if polarization was the only effect on diffraction efficiency being varied, the 0 degree and 90 degree rotations should have very similar diffraction efficiency versus time profiles, as should the 20 degree and 70 degree, and the 40 degree and 50 degree. However, from Figure 7 one can see that the diffraction efficiencies for all angles less than the bisector angle (45 degrees) are higher than for those angles greater than 45 degrees. When the polarizer is aligned at 0 degrees, the striations in the plastic create a horizontal 'cigar shaped' distribution of light in the hologram plane. At 90 degrees, the distribution of light is vertical. Apparently, the horizontal distribution acts to significantly enhance diffraction efficiency by enforcing the original grating during reading. As the distribution moves towards a vertical orientation, the diffraction efficiency enhancement is much less apparent.

2.6 Conclusion

Diffuse Fourier transform holograms were successfully recorded and 'played back'. Experiments were performed to identify critical recording parameters in an attempt to optimize the holographic diffraction efficiency of the holograms. It was found that the diffraction efficiency remained relatively high for reference to object beam angular separations of approximately 15 to 35 degrees. A reference beam to object beam power ratio of six to one provided the largest diffraction efficiency. In terms of total power incident on the crystal during recording, the diffraction efficiency increased with increasing power up to 36.5 mW, at which point further increases in incident power resulted in decreasing diffraction efficiency. Undesired

scattering off of the grating at these higher powers is believed to be the cause of the decreasing diffraction efficiencies. As theoretically predicted, diffraction efficiencies were maximized when using extra-ordinarily polarized read beams.

One unexpected, yet beneficial, result occurred as a result of using the plastic anisotropic diffuser. Preliminary experiments have shown the holographic diffraction efficiency increases during illumination of the hologram by the object beam when the diffuser is present in the beam path. This increasing diffraction efficiency is believed to result from internal gratings present in the plastic diffuser. As the diffraction efficiency increased, the resolution of the diffracted beam became slightly distorted. However, the increase in diffracted beam power will be most beneficial during operation of the Holographic Associative Memory. The next chapter develops the theory describing operation of the HAM.

III. Theory of a Holographic Associative Memory Using Non-Linear Storage Media

3.1 Introduction

This chapter develops the theory of operation for a holographic associative memory which uses non-linear material for both holographic storage and phase conjugation. The equations developed will be based on the storage of multiple objects within the holographic medium. The architecture is that of a single iteration system, meaning there is only one 'pass' of the (distorted) input through the storage medium.

As a result of using a dynamic storage medium, other gratings are written in addition to the desired holographic grating. As stated by Gunter, "recording of such [volume] holograms permits the interference of an incident light beam with its own diffracted beam inside the recording material. This effect causes the continuous recording of a new grating ..." (14:219). Additionally, internal reflections (within the lithium niobate crystal) interfering with the input object beam, as well as the coupling of the phase conjugate return beam, the distorted input beam, and the original hologram, create gratings which generate additional wavefronts. The equations describing the formation of the grating due to the coupling of the PCR, the input object beam, and the original grating are developed in Appendix A.

3.2 Single Iteration System Architecture

The HAM developed and implemented is a single iteration system. This 'single pass' system allows only one correlation of the input with the stored objects. The image quality of the associated output is thus a function of the degree of correlation obtained, during this single pass, between the distorted input and the stored objects. Figure 2 illustrates the architecture for the HAM.

The key components of the system are the $LiNbO_3$ crystal, which serves as the holographic memory, and the $BaTiO_3$ crystal, which acts to temporally phase conjugate the wavefront resulting from the correlation of the distorted input with the stored objects. This phase conjugate 'auto-reference' beam re-illuminates the holcgram, generating the holographic associative memory output. Because the desired output image results from the phase conjugate beam illuminating the hologram, from here forward it will be referred to as the 'phase conjugate image'. The $LiNbO_3$ crystal used is the same iron doped crystal described in Chapter Two. The phase conjugator is a single domain, 5 x 5 x 3 mm^3, $BaTiO_3$ crystal with the c-axis parallel to one of the 5 mm edges.

3.3 Theory of Operation

The first step in the operation of the HAM is to holographically record the objects to be stored. Chapter Two developed the general equations describing the storage of a single object in non-linear holographic media, such as lithium niobate. The following development for the storage of multiple objects parallels Chapter Two, as well as Fielding's work (9:7).

Let $e_o^m(\vec{r},t)$ represent the m^{th} input object in the space domain (x,y,z) [input plane] and $E_r^m(f_x,f_y)\exp^{i(\omega t-2\pi(\alpha_m f_y+\beta_m f_z))}$ represent its unique Gaussian amplitude plane wave reference in the Fourier domain (f_x,f_y,f_z) [hologram plane], at spatial frequencies $\alpha_m = \sin\theta_m/\lambda$ and $\beta_m = \cos\theta_m/\lambda$. θ_m is the angle between the object and reference waves, as shown in Figure 8. The optical frequency is ω.

The total complex field incident on the crystal is the sum of the object and reference beams:

$$E^m(f_x,f_y) = E_o^m(f_x,f_y) + E_r^m(f_x,f_y)\exp^{i(\omega t-2\pi(\alpha_m f_y+\beta_m f_z))} \qquad (21)$$

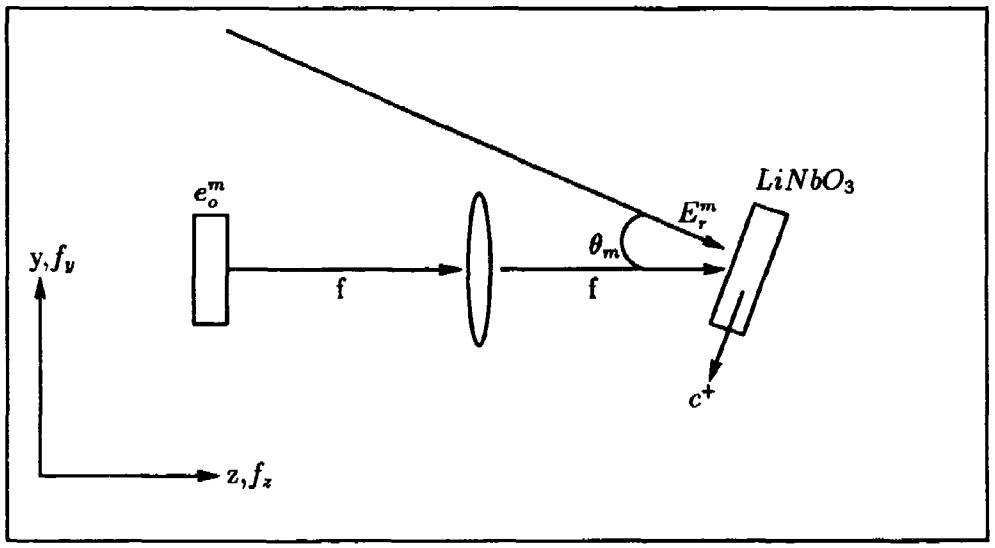

Figure 8. Hologram Recording of Multiple Objects

$E_o^m(f_x, f_y)$ is the Fourier transform of $e_o^m(\vec{r}, t)$, which is illuminated by a plane wave and transformed by the lens in Figure 8.

As in Chapter Two, the refractive index modulation in the crystal responds to the *intensity* variation of the total field within the crystal:

$$I(f_x, f_y) = \sum_m |E_m(f_x, f_y)|^2 \tag{22}$$

$$= \sum_m \left| E_o^m(f_x, f_y) + E_r^m(f_x, f_y) \exp^{i(\omega t - 2\pi(\alpha_m f_y + \beta_m f_z))} \right|^2 \tag{23}$$

Following the development in Chapter Two for a phase grating, the complex transmittance of the grating is given by

$$T_p(f_x, f_y) = \sum_m \exp^{i\gamma^m I(f_x, f_y)} \approx 1 + i \sum_m \gamma^m I(f_x, f_y) \tag{24}$$

γ^m is shown to be a function of m since the refractive index modulation (and hence the diffraction efficiency) of the gratings decreases as the number of objects stored

increases. This is because each successive recording tends to erase the previous gratings. In practice, this effect can be compensated by "progressively decreasing the exposure during the recording sequence" (28:183). Substituting for $I(f_x, f_y)$ from above

$$T_p(f_x, f_y) \approx 1 + i \sum_m \gamma^m |E^m(f_x, f_y)|^2 \quad (25)$$

$$\approx 1 + i \sum_m \gamma^m \left| E_o^m(f_x, f_y) + E_r^m(f_x, y) \exp^{i(\omega t - 2\pi(\alpha_m f_y + \beta_m f_z))} \right|^2 \quad (26)$$

Dropping the (f_x, f_y) notation and the temporal dependence (because it has no impact on the formation of the phase grating)

$$T_p \approx 1 + i \sum_m \gamma^m \left[|E_o^m|^2 + |E_r^m|^2 + E_o^m E_r^m \exp^{+i2\pi(\alpha_m f_y + \beta_m f_z)} + E_o^{m^*} E_r^m \exp^{-i2\pi(\alpha_m f_y + \beta_m f_z)} \right] \quad (27)$$

where $E_o^{m^*}$ represents the spatial complex conjugate of the object wave. Equation 27 defines the complex transmittance for m objects stored in the non-linear holographic media.

The system is now presented with an incomplete or distorted version of one of the stored objects, $\hat{e}_o^{mo}(x, y)$, whose Fourier transform is $\hat{E}_o^{mo}(f_x, f_y)$. The equation describing the output from the hologram when a distorted object is incident upon the grating is given by

$$A_t(f_x, f_y) = \hat{E}_o^{mo}(f_x, f_y)\, T_p(f_x, f_y) \quad (28)$$

Dropping the (f_x, f_y) notation and expanding

$$A_t = \hat{E}_o^{mo} \left[1 + i \sum_m \gamma^m \left(|E_o^m|^2 + |E_r^m|^2 + E_o^m E_r^m \exp^{+i2\pi(\alpha_m f_y + \beta_m f_z)} + E_o^{m^*} E_r^m \exp^{-i2\pi(\alpha_m f_y + \beta_m f_z)} \right) \right] \quad (29)$$

$$
\begin{aligned}
&= \hat{E}_o^{mo} + i\hat{E}_o^{mo}\sum_m \gamma^m |E_o^m|^2 + i\hat{E}_o^{mo}\sum_m \gamma^m |E_r^m|^2 \\
&\quad + i\hat{E}_o^{mo}\sum_m \gamma^m E_o^m E_r^m \exp^{+i2\pi(\alpha_m f_y + \beta_m f_z)} \\
&\quad + i\hat{E}_o^{mo}\sum_m \gamma^m E_o^{m^*} E_r^m \exp^{-i2\pi(\alpha_m f_y + \beta_m f_z)}
\end{aligned} \tag{30}
$$

The only term of interest in Equation 30 is the fifth term, representing the first diffracted order, which propagates towards the phase conjugate mirror. The first three terms are 'DC' zero order components which travel along the input object beam direction. The fourth term does not propagate because of phase mismatch, which arises when the Bragg angle requirements are not satisfied in thick holographic media (8:36). Ignoring the first four terms, the fifth term can be expanded as follows:

$$
\begin{aligned}
A_t &= \underbrace{i\gamma^{mo}\hat{E}_o^{mo}E_o^{mo^*}E_r^{mo}\exp^{i(\omega t - 2\pi(\alpha_{mo}f_y + \beta_{mo}f_z))}}_{Scaled\ "Auto-Reference"} \\
&\quad \underbrace{+ i\hat{E}_o^{mo}\sum_{m\neq mo}\gamma^m E_o^{m^*}E_r^m \exp^{i(\omega t - 2\pi(\alpha_m f_y + \beta_m f_z))}}_{Cross-Reference\ Noise}
\end{aligned} \tag{31}
$$

When a distorted input $\hat{E}_o^{mo}$ closely resembles the stored object E_o^{mo}, the first term of Equation 31 will be a close recreation of the original reference beam used to record the hologram.

Equation 31 is then focused by the Fourier transform lens of Figure 2 onto the $BaTiO_3$ phase conjugate mirror (PCM). The PCM performs a non-linear threshold (NL) and phase conjugates the strongest component from Equation 31. The component which is phase conjugated should be the first term, since it represents an auto-correlation of the distorted input with its stored, undistorted version. The temporal phase conjugation, denoted by $^{\odot}$ in the equations below, causes the auto-reference wavefront to travel back exactly along its original path. The general form

of the phase conjugate return is given by

$$NL\left[F\left(i\hat{E}_o^{mo}\sum_m \gamma^m E_o^{m^*} E_r^m \exp^{i(\omega t - 2\pi(\alpha_m f_y + \beta_m f_z))}\right)\right]^{\circledcirc} \tag{32}$$

The wavefront represented by Equation 32 is Fourier transformed as it propagates back towards the holographic medium. The initial output from the hologram when illuminated by this Fourier transformed, phase conjugated auto-reference wavefront is described by the product of Equation 32 and the transmission grating, Equation 27. Let $A_t'(f_x, f_y)$ represent the initial output:

$$A_t' = F\left[NL\left(F\left[i\hat{E}_o^{mo}\sum_m \gamma^m E_o^{m^*} E_r^m \exp^{i(\omega t - 2\pi(\alpha_m f_y + \beta_m f_z))}\right]\right)^{\circledcirc}\right] T_p \tag{33}$$

Expanding T_p and performing the multiplication generates five terms. The first three terms represent wavefronts which travel along the phase conjugate return direction. The fourth term travels back towards the distorted input, representing the wavefront containing the 'phase conjugate' image. The fifth term does not propagate because the phase match condition (associated with the Bragg angle requirement) is not satisfied. The five terms are shown (in the order discussed) below:

$$\begin{aligned} A_t' \;=\; & F\left[NL\left(F\left[i\hat{E}_o^{mo}\sum_m \gamma^m E_o^{m^*} E_r^m \exp^{i(\omega t - 2\pi(\alpha_m f_y + \beta_m f_z))}\right]\right)^{\circledcirc}\right] \\ & \left(1 + i\sum_n \gamma^n \left[|E_o^n|^2 + |E_r^n|^2\right]\right) \\ & + F\left[NL\left(F\left[i\hat{E}_o^{mo}\sum_m \gamma^m E_o^{m^*} E_r^m \exp^{i(\omega t - 2\pi(\alpha_m f_y + \beta_m f_z))}\right]\right)^{\circledcirc}\right] \\ & \left[i\sum_n \gamma^n E_o^n E_r^n \exp^{+i2\pi(\alpha_n f_y + \beta_n f_z)}\right] \\ & + F\left[NL\left(F\left[i\hat{E}_o^{mo}\sum_m \gamma^m E_o^{m^*} E_r^m \exp^{i(\omega t - 2\pi(\alpha_m f_y + \beta_m f_z))}\right]\right)^{\circledcirc}\right] \\ & \left[i\sum_n \gamma^n E_o^{n^*} E_r^n \exp^{-i2\pi(\alpha_n f_y + \beta_n f_z)}\right] \end{aligned} \tag{34}$$

The phrase 'initial' was used above to highlight the nature of using a dynamic recording medium. Specifically, the phase conjugate auto–reference beam incident upon the non–linear holographic medium couples with both the incoming distorted object beam and the original holographic grating to form a 'secondary' grating. This secondary grating creates additional diffracted wavefronts which are experimentally observed. The equations describing the formation and illumination of this 'secondary' grating are developed (for a single stored object) in Appendix A. Experimental observations of this phenomenon are discussed in the next chapter.

The fourth term of Equation 34 undergoes another Fourier transform, which generates the term below:

$$NL\left(F\left[i\hat{E}_o^{mo}\sum_m \gamma^m E_o^{m^*} E_r^m \exp^{i(\omega t-2\pi(\alpha_m f_y+\beta_m f_z))}\right]\right)^{\odot}$$

$$* F\left[i\sum_n \gamma^n E_o^n E_r^n \exp^{+i2\pi(\alpha_n f_y+\beta_n f_z)}\right] \tag{35}$$

The only wavefront which travels back towards the input object occurs when the indices of summation are equal, $m = n$. For this case, Equation 35 becomes

$$NL\left(F\left[i\hat{E}_o^{mo}\gamma^m E_o^{m^*} E_r^m \exp^{i(\omega t-2\pi(\alpha_m f_y+\beta_m f_z))}\right]\right)^{\odot}$$
$$*F\left[i\gamma^m E_o^m E_r^m \exp^{+i2\pi(\alpha_m f_y+\beta_m f_z)}\right] \tag{36}$$

Defining $E_r^m \exp^{-i2\pi(\alpha_m f_y+\beta_m f_z)}$ as R^m, whose Fourier transform is r^m, leads to

$$NL\left(F\left[i\hat{E}_o^{mo}\gamma^m E_o^{m^*} R^m \exp^{i\omega t}\right]\right)^{\odot} * \bar{F}\left[i\gamma^m R^{m^*} E_o^m\right] \tag{37}$$

Assuming the $BaTiO_3$ crystal performed the non–linear threshold on only the reference associated with the auto–correlation term, and using the properties of Fourier

transforms, convolutions, and correlations, Equation 37 becomes

$$F\left(\left[i\hat{E}_o^{mo}\gamma^{mo}E_o^{mo^*}R^{mo}\exp^{i\omega t}\right]^{\odot}\left[i\gamma^{mo}R^{mo^*}E_o^{mo}\right]\right) \tag{38}$$

which leads to the output of the associative memory, $\tilde{e}_o^{mo}$:

$$\tilde{e}_o^{mo} = \exp^{i\pi}(\gamma^{mo})^2\left[(\hat{e}_o^{mo} * e_o^{mo}) * r^{mo}\right] * r^{mo} * e_o^{mo} \tag{39}$$

When $\hat{e}_o^{mo} \approx e_o^{mo}$, then the correlation will have a large, narrow peak and the output will be a recreation of the original stored object, e_o^{mo}.

3.4 Effects of Using Dynamic Storage Medium

The $Fe{:}LiNbO_3$ crystal is a dynamic medium which can form gratings whenever two beams intersect within the crystal. Therefore, additional gratings (other than the desired holographic grating) are formed in the medium during HAM system operation. As previousiy mentioned, one of these gratings is formed when the PCR, the distorted object beam, and the original grating interfere. The equations describing this 'secondary' grating are developed in Appendix A.

As Chapter Two describes, maximum diffraction efficiency is obtained when the normal to the c^+ axis of the $Fe{:}LiNbO_3$ crystal bisects the angle between the reference and object beams. This orientation, however, allows the reference's Fresnel reflection off of the highly polished crystal to travel exactly back along the object beam direction. This reflection is therefore focused on the object transparency by the Fourier transform lens. The focused spot then reflects normally off of the transparency and, as a result, adds noise to the object beam entering the crystal. Ensuring that the plastic diffuser attached to the object transparency is facing towards the crystal helps to minimize this noise, but the reflection is still bright enough to significantly 'wash out' the input object.

For purposes of this research, the problem was avoided by rotating the crys-

tal such that the reference reflection missed the Fourier transform lens. Thus, the noise never entered the system. The relative impact on achievable diffraction efficiency due to this 'non–optimum' crystal orientation was minimal, when compared to environmental disturbances (such as thermal fluctuations and table vibrations). A more desirable solution, which would allow for optimum crystal alignment, would be to immerse the crystal in a index matching liquid gate to remove the unwanted reflection.

Another drawback of rotating the crystal, in addition to reducing the achievable diffraction efficiency, is that internal reflections resulting from refractive index 'boundaries' are still present and can interact with other beams to form unwanted gratings. One such grating is formed by the intersection of the input object beam and the reflection of the reference beam off of the 'back' side of the crystal. Specifically, the reference beam enters the crystal and travels through to the 'back' side. Because of the differences in index of refraction at this boundary, a portion of the reference beam is internally reflected back through the crystal. It is the interaction of this internal reflection and the distorted input object wave which generates the unwanted grating.

Empirical evidence obtained during experimentation with the HAM system supports the presence of this grating. Before a phase conjugate return is generated, a reflection in the reference's Fresnel reflection direction is obtained when the system is illuminated by the distorted object beam. This reflection can only be explained by the presence of an undesired grating. In addition, as the PCR begins to illuminate the hologram, four additional beams are observed leaving the $Fe{:}LiNbO_3$ crystal.

Two of these beams result from the PCR interacting with the original grating. The first, and most important, is the PCR's first order diffraction off of the original grating. This beam is the desired HAM output. The second beam travels back towards the reference, representing the zero order (DC) transmission of the PCR through the original grating.

The third and fourth beams result from the internal reflection of the PCR illuminating the unwanted internal reflection grating. The third beam is the zero order diffraction of the PCR's internal reflection traveling through the unwanted internal reflection grating. This beam is basically a 'continuation' of the PCR. The fourth beam, however, is a replica of the input object beam. Hence, it is the first order diffraction term resulting from the reflected PCR illuminating the unwanted grating.

The location and spatial content of these last two beams, as well as the object beam reflection described above, can only be explained by the presence of this second grating. Figure 9 is a diagram of the relative location of each of the beams discussed. Beams one through four are those described above, beam five represents the object's reflected beam in the reference's Fresnel reflection direction, and the sixth and seventh beams represent the zero order and first order terms, respectively, from the object wave illuminating the original hologram. For the figure, the crystal was orientated such that the normal to the c^+ axis of the $Fe{:}LiNbO_3$ crystal was approximately six degrees away from the reference beam, but still between the reference and object beams. This orientation ensured the reference beam's Fresnel reflection did not fall upon the Fourier transform lens. In subsequent experiments, rotating the crystal (before recording) caused the third and fourth beams described above to rotate in a predictable manner. For example, when the crystal was aligned such that the normal to the c^+ axis bisected the angle between the reference and object beams, the beams overlapped the zero and first order diffracted beams generated by the distorted input object illuminating the original grating (beams six and seven in Figure 9). Also, the angular separation between beams three and four, and between beams six and seven, remained constant and equal to the angular separation between the reference and object beams used to record the original hologram.

The last piece of empirical evidence which supports the presence of this particular unwanted grating involves the effect of blocking the phase conjugate return on

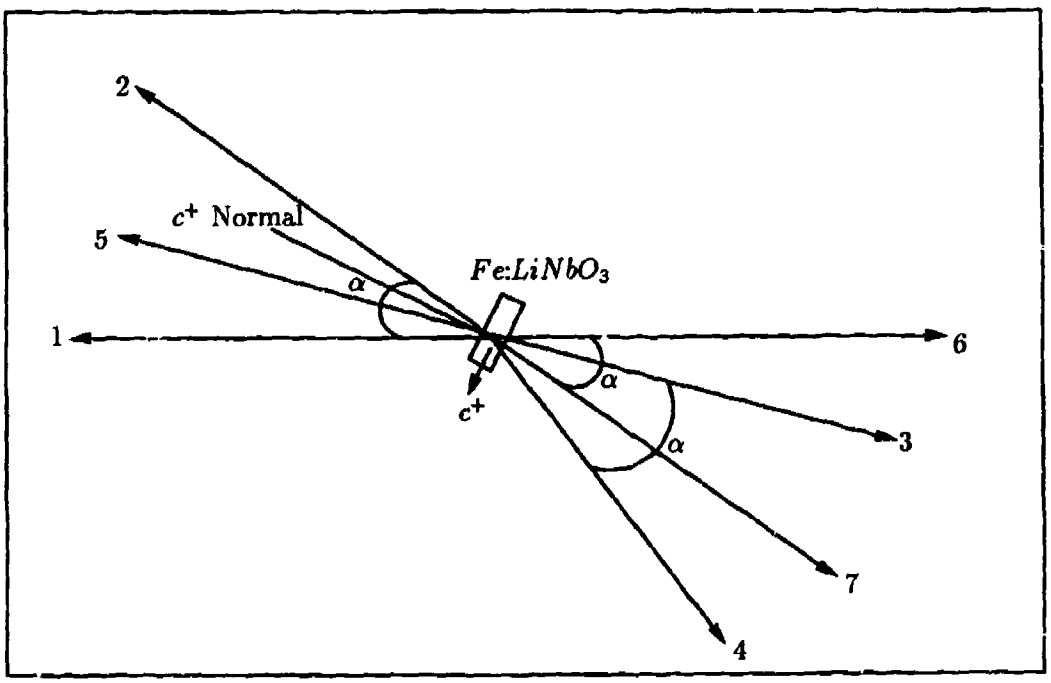

Figure 9. Wavefronts Present During HAM Operation

the aforementioned beams. As expected, blocking the PCR causes the HAM image and the beam travelling towards the reference to vanish. In addition, blocking the PCR causes beams three and four to also vanish. Thus, these beams are indeed generated by the PCR illuminating the unwanted grating.

3.5 Conclusion

This chapter described the operational theory of a holographic associative memory which uses a dynamic, non-linear storage medium. Equation 39 shows that a complete, undistorted output will theoretically be generated by the HAM when a distorted version of one of the stored images is input to the system.

In addition, empirical evidence was presented which supports the conclusion that additional gratings are generated within the medium as a result of coupling be-

tween internal reflections and incident beams. Relevant equations were developed to provide a (supporting) theoretical explanation for the existence of these additional gratings. These unwanted gratings diffract the beams incident on the system's memory such that numerous beams are produced. While these extraneous beams tend to complicate the detailed explanation of system operation, understanding the manner in which they are generated is not relevant to the operation of the HAM. These additional beams have little impact on overall system performance (aside from diffracting some energy away from the HAM output). In fact, if the unwanted gratings significantly reduced the phase conjugate image intensity, they could be eliminated by immersing the memory element in a index matching liquid gate.

The next chapter describes experimental results of operating the HAM. Initial experiments investigate performance with a single stored object, and then the system is tested in the more realistic environment of recalling a specific object from several stored objects.

IV. Holographic Associative Memory Experiments Using $Fe{:}LiNbO_3$

4.1 Introduction

The previous chapter provided the theoretical development of a Holographic Associative Memory which uses non-linear, dynamic holographic storage media. This chapter describes the implementation of that theory in a single iteration HAM system. Specifically, the procedures used and the results obtained during experimentation with the HAM system of Figure 2 are discussed.

Initial experiments involved the storage and subsequent recall of a single object. Effects on system performance due to input object distortion were qualitatively investigated by blocking portions of the input and observing the resulting HAM output. The next set of experiments involved the storage of multiple objects, using angular multiplexed holography, and subsequent recall of a particular stored object from its associated input.

The chapter begins with a discussion of the procedures followed in both sets of experiments and concludes with the presentation and analysis of the results obtained.

4.2 Experimental Procedures

The first step in operating the HAM requires the storage of two dimensional image(s) holographically. The first set of experiments involved the storage of a single object. The object used was the Air Force resolution chart–plastic diffuser combination described in Chapter Two. Beam polarization, beam powers, duration of exposure, and the ratio of reference beam to object beam power were all chosen to optimize the recording process, based upon the holography results of Chapter Two. However, to avoid the noise from the reference beam's Fresnel reflection (described in Chapter Three), the normal to the $Fe{:}LiNbO_3$ crystal's c^+ axis was aligned

approximately six degrees from the reference beam, but still between the reference and object beams.

Once the hologram was stored, the reference beam was blocked and the hologram illuminated with a distorted version of the stored object. The distortion was achieved by blocking a percentage of the area of the original object transparency. The output beam travelling in the original reference beam direction is Fourier transformed by the lens in Figure 2. The resulting beam is allowed to expand slightly by placing the $BaTiO_3$ crystal just beyond the back focal plane of the lens, in order to facilitate beam fanning within the $BaTiO_3$ crystal. The crystal is located such that the input beam travels through the crystal and reflects off the back corner (reference the self pumped phase conjugation photograph in Fielding's thesis) (9:27).

This reflection off of the corner generates the two coupled interaction regions within the crystal required to initiate self-pumped phase conjugation. The phase conjugate return (PCR) then leaves the $BaTiO_3$ and travels exactly back along the reference beam direction. The Fourier transform of the PCR illuminates the hologram. The resulting HAM image is separated from the distorted input object beam by the beam-splitter in Figure 2.

The above procedure is modified slightly for the storage and recall of multiple objects. To begin, each object is stored with a reference beam of unique direction. Based upon Gaylord's results concerning the angular selectivity of holograms in $LiNbO_3$, each reference beam should be separated by at least 0.4 degrees (measured externally) (11:4773). To ensure crosstalk between stored objects does not occur in this proof of concept experiment, each reference beam was separated by an angle of 3.0 degrees. The reference beam direction was changed by mounting the reference beam mirror (reference Figure 4) on a translational stage and moving the mirror for each successive recording. Two tactical target transparencies and an Air Force resolution chart were stored. A plastic diffuser similar to the one used in the holography experiments of Chapter Two was attached to each object transparency.

Once the objects were stored, a particular input object beam was allowed to illuminate the $Fe:LiNbO_3$ crystal. The $BaTiO_3$ crystal was adjusted to support beam fanning and phase conjugation of the strongest beam leaving the hologram in the general direction of the reference beams used to store the objects. The strongest beam hopefully corresponds to the correlation of the input with its associated stored object, as described in Chapter Three. After the system generates the HAM image associated with that input, the input transparency is removed and a transparency of one of the other stored objects is inserted in the object beam path. The process is then repeated.

4.3 Experimental Results

The first experiment involved the storage of a single object, the Air Force resolution chart. Figure 10 is a photograph of the complete, undistorted object which was stored in the $Fe:LiNbO_3$ crystal. The photograph was taken by focusing the object wavefront on a white card, without the holographic medium in place.

As a check of the quality of the recording, the hologram was illuminated with the reference beam and the resulting diffracted image inspected. The grating was illuminated quickly with a low level intensity reference beam in order to minimize grating erasure. The resulting hologram was of excellent quality, as Figure 11 demonstrates. This photograph was taken by focusing the diffracted image, generated by the incident reference beam, onto a white card. The resolution of the holographic image was measured to be approximately 16 *l/mm*. This resolution was limited by the input and output image optical components, and does not represent a limit to the resolution of the iron doped lithium niobate.

The reference beam was then blocked and the power in the object beam maximized. As a result of the internal étalon, the maximum power obtained from the argon ion laser through the object transparency was approximately 18.0 mW. For the first attempt at complete, single iteration system operation, the input trans-

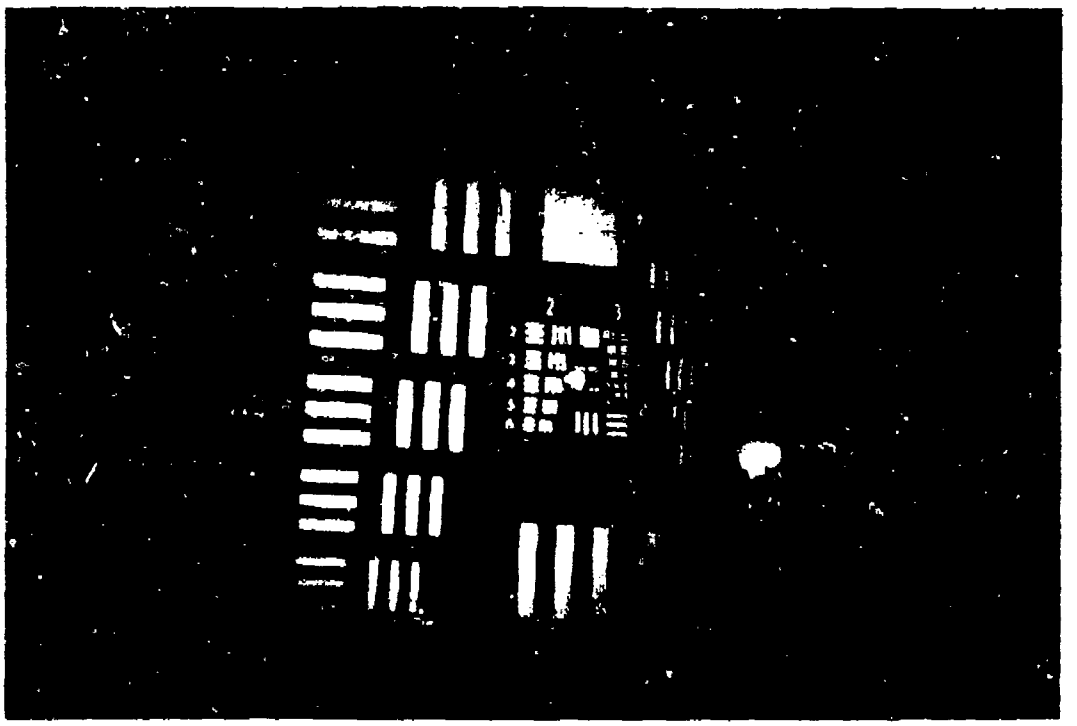

Figure 10. Object Stored in Holographic Memory

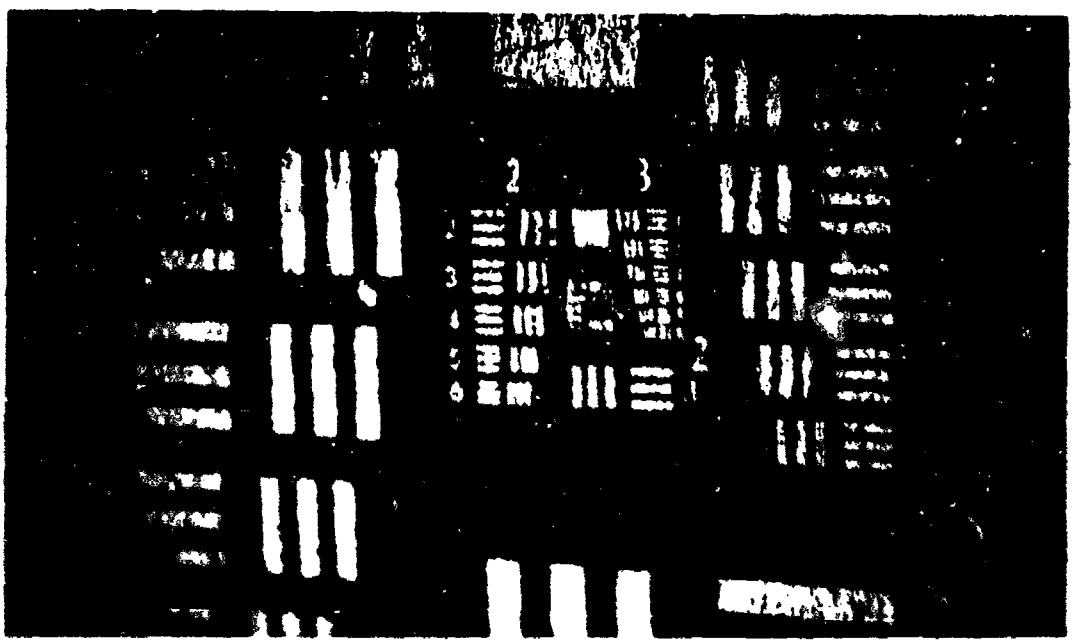

Figure 11. Typical Holographic Image (Magnified)

parency was not distorted. Thus, a complete object beam of approximately 18.0 mW illuminated the hologram. The $BaTiO_3$ crystal was adjusted (as described in the previous section) and beam fanning began within the phase conjugate mirror. Within three minutes, the phase conjugate return had sufficiently illuminated the holographic grating to begin forming the 'phase conjugate' image. The power in the diffracted beam entering the $BaTiO_3$ crystal after these first three minutes had risen to 0.5 mW, from an initial value of 0.3 mW. As expected, the increasing diffraction efficiency of the hologram, described in Chapter Two, significantly contributes to the formation of the phase conjugate image.

At first, the phase conjugate image was incomplete, exhibiting a gradual fading around the extreme edges of the resolution chart. However, after approximately five minutes from the time it first appeared, the phase conjugate image was completely filled. It was observed that a typical HAM output image lasted for about forty minutes, by which time the grating had degraded enough to make the image nearly unresolvable. Figure 12 is a photograph of a typical phase conjugate image after eleven minutes of operation. The inversion of the image is due to a focusing lens. The resolution of the image was measured to be approximately 16 *l/mm*, and was limited by the optics used to magnify and focus the output image.

Once the basic operation of the system was verified, the next step was to investigate the HAM's performance when presented with a distorted input. Figure 13 is a photograph of the distorted Air Force resolution chart. Approximately 25 percent of the original object (part of group 5 and all of group 6) has been blocked.

Following the same procedure as above, the conjugate image was formed. As in the previous case, the image began to form in about three minutes. However, the area of the original object which was removed never approached the level of brightness of the unblocked portion. After about eight minutes, the blocked portion was barely discernable to the naked eye, but as Figure 14 shows, the camera could not detect this region.

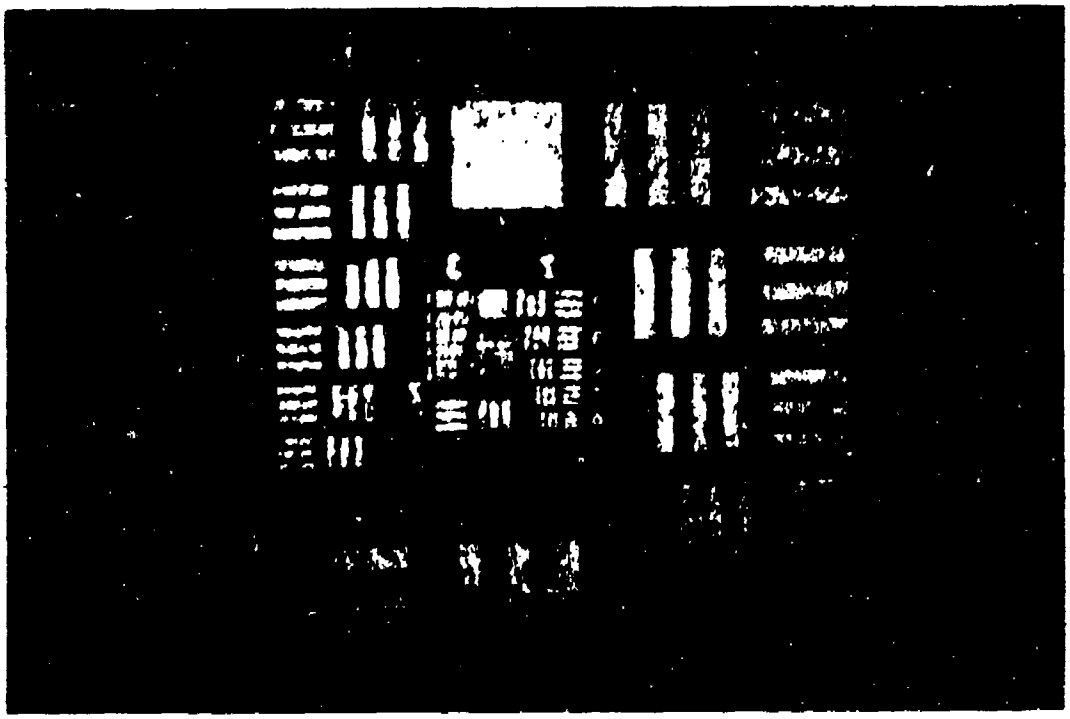

Figure 12. Typical Output Image from a Single Iteration Ham System

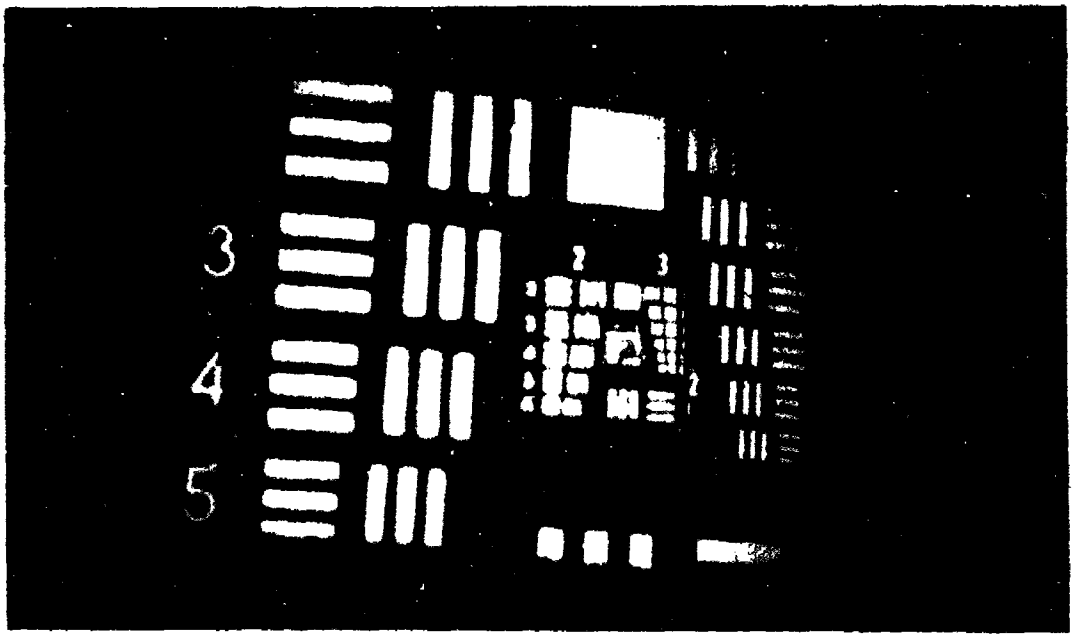

Figure 13. Distorted Input Object

Figure 14. Ham Output when Presented with a Distorted Input

A possible explanation for the lack of complete image recall when presented with the distorted input could be linked to the single iteration architecture of the system. Apparently the single correlation of the distorted input with the objects stored in memory is not sufficient to create a satisfactory replica of the original reference beam. As a result, the phase conjugate return does not generate a complete image when iliuminating the holographic grating. The addition of another $BaTiO_3$ crystal in the object leg of the system could be used to phase conjugate the HAM's output, thus forming a closed loop, full resonant cavity. A full resonant cavity would allow multiple correlations of the distorted object wave with the stored object(s), which should enhance the generation of a complete output image. Chapter Five addresses this full resonant architecture in more detail.

Upon completion of the single stored object experiments, multiple objects were stored to investigate the HAM system's performance under a more realistic environment. To minimize erasure of each hologram during the reference angle multiplexed

recording, the objects were stored in a sequence based on the amount of energy transmitted by each transparency. Specifically, the object transparency which transmitted the most energy was stored first, the transparency which transmitted the next highest amount of light was stored second, and the transparency blocking the most light was stored last.

The first transparency, a dark tank on a clear background, was stored at a reference to object beam angle of 28 degrees. The second object, a transparency of three dark tactical targets (F–15, tank, and truck) on a clear background, was stored at an angle of 31 degrees (reference Mayo's research for photographs of these objects (20)). The final object, the Air Force resolution chart used previously, was stored at an angle of 25 degrees. In each case, the reference to object beam angle was changed by moving only the reference beam. The object beam and the crystal were not disturbed. The exposure was held constant at 60 seconds for each of the three recordings. The diffraction efficiencies of the three holograms were in the 1 to 5 percent range, with each successive hologram demonstrating a slight decrease in efficiency. Each diffraction efficiency was measured immediately after recording (before the next hologram was written) by blocking the reference beam and measuring the ratio of diffracted object beam power to input object beam power.

Each successive object slide reduced the energy in the object beam by approximately 40 percent. It was felt this reduction in energy would be enough to allow multiple recording without erasing previous gratings. This was not the case, however. Attempts to re-illuminate the first and second holograms with either the associated reference or object beam failed to generate a diffracted beam. Several attempts at multiple recording were made. In each case, previous holograms were significantly erased by the writing of additional holograms. Apparently, the successive decrease in object beam energy for each hologram written was not large enough to minimize erasure.

In an attempt to further minimize the erasure process during the recording of

additional holograms, the exposure time was reduced for each successive recording. The objects were still recorded in order of decreasing transmitted energy. The first hologram was recorded with an exposure of 60 seconds, the second was recorded for 40 seconds, and the last hologram was written for 20 seconds. The resulting diffraction efficiency for the first hologram was in the 2 to 5 percent range, the second hologram's diffraction efficiency fell to the 0.5–2.0 percent range, and the last hologram had a diffraction efficiency of less than 1.0 percent.

All three holograms were easily illuminated with the reference beam by merely moving the reference beam to the correct angular position. In addition, illumination of the hologram with any of the object wavefronts (after careful replacement of the object transparency) produced a correlation beam leaving the hologram in the direction of the associated reference beam. The presence of weaker correlation beams, corresponding to the correlation of the input object with the different stored objects, were not observed at this time.

The reduction in exposure length for each successive recording minimized erasure of the previous gratings. Thus, each hologram was still present in the crystal and capable of being 'read out' by either the associated object or reference beam. With the storage of multiple objects using reference angle multiplexing accomplished, the next step was to attempt to form the 'phase conjugate' image for each of the objects stored in memory.

After the three holograms were written, the first object slide was carefully re-inserted in the object beam path. The diffraction efficiencies of these three holograms were not measured in order to minimize grating erasure. The object beam was allowed to illuminate the $Fe{:}LiNbO_3$ crystal and the object slide location adjusted to maximize the resulting correlation peak leaving the crystal. The object beam power was increased such that the correlation beam had an initial power of approximately 0.3 mW. The correlation beam illuminated the $BaTiO_3$ crystal, which was adjusted to support beam fanning and self-pumped phase conjugation. After approximately

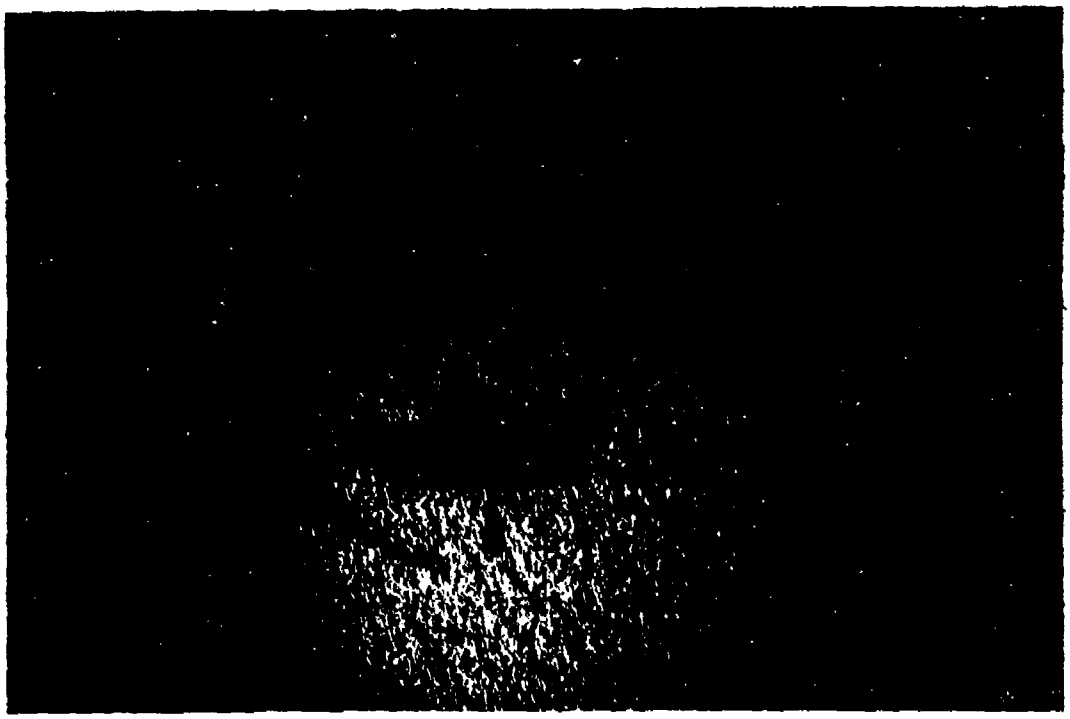

Figure 15. Ham Output when Presented with First Object Stored

five minutes, the phase conjugate image appeared. The image was allowed to build for approximately ten minutes and then the object beam incident on the hologram was blocked. Figure 15 is a photograph of the phase conjugate image during the first minute of its formation. This photograph was taken at the output plane identified in Figure 2. The reconstruction of this stored object clearly demonstrates the system's ability to recall a particular object from several stored objects. In fact, by recalling the *first* object stored, the system has reconstructed an image from the weakest stored hologram due to hologram erasure during recording of subsequent gratings.

The second object slide was carefully aligned in the object beam path to maximize the resulting correlation beam. A secondary correlation wavefront, much more diffuse than the desired correlation peak, was now present. This diffuse wavefront propagated in the direction of the first object's reference beam. The $BaTiO_3$ was adjusted to generate the phase conjugate return of the desired correlation peak. The adjustment amounted to a lateral translation of approximately 2 mm. The second

correlation beam, however, was weaker than the first object's correlation peak. As a result, beam fanning in the phase conjugate mirror did not begin for nearly three minutes. The phase conjugate return was never generated and the phase conjugate image did not form. Attempts to form the phase conjugate image of the third object also failed.

It was felt that too much time had been spent observing the first object's phase conjugate image. The gratings associated with the second and third objects had been partially erased by the input object beam and the phase conjugate return, which significantly decreased their diffraction efficiencies. Thus, the resulting correlation peaks were too weak to allow the $BaTiO_3$ to form the phase conjugate returns.

Three new holograms were written, as before, and the first object slide re-inserted in the object beam. The phase conjugate image was generated in approximately three minutes and the object beam blocked twenty seconds later. The second object replaced the first in the object beam, and the wavefront was allowed to illuminate the holograms. The correlation peak was still weak compared to the first object's correlation peak. Again, no phase conjugate image was formed. Attempts to form the third object's phase conjugate image were also unsuccessful.

In an attempt to expedite the formation of the phase conjugate return, the z-cut $BaTiO_3$ crystal used thus far in the experiments was replaced with a 45 degree cut, 5 x 5 x 3 mm^3, single domain crystal. According to Wilson, the response time and phase conjugate reflectivity of 45 degree cut $BaTiO_3$ is better than z-cut crystals (31:61). The three holograms were again recorded and the first object transparency placed in the object beam path to maximize the correlation peak. To maximize the phase conjugate return, the 45 degree cut crystal was orientated such that the angle between the surface normal and the incoming beam was 40 degrees, based on experimental results obtained by Wilson (31:96). Beam fanning was evident immediately upon illumination by the correlation peak. A phase conjugate image was formed within two minutes. Typical response times for the z-cut crystal's phase

conjugate return were three to five minutes. Therefore, the 45 degree cut did improve the system's response time. The object beam was immediately blocked, and the second object transparency inserted in the object beam path. Again beam fanning in the 45 degree cut $BaTiO_3$ was immediate. However, no phase conjugate image was generated. The third object slide was inserted into the object path, but no phase conjugate image was formed.

Several attempts were made to generate multiple phase conjugate images, but in all cases the results were the same. With 'fresh' holograms, any one of the three objects could be inserted into the object beam path and its associated phase conjugate image generated. However, once one phase conjugate image was produced, the gratings present in the iron doped $LiNbO_3$ crystal became distorted enough to not allow the formation of any other phase conjugate images. Apparently, the combined effects of illuminating the dynamic holographic medium with the bright input object beam and the phase conjugate return are enough to significantly distort the original gratings. Perhaps an alternative approach, using permanently stored holograms (via thermal cycling), would eliminate this effect and allow the generation of multiple phase conjugate images. A system which cyclically rewrites the desired holographic gratings in memory between each object recall could also provide a workable alternative to the grating distortion problem.

4.4 Conclusion

This chapter described experimental results obtained during operation of the single iteration HAM system. Experimental procedures defining system operation for both single and multiple stored object(s) were identified. Initial experiments verified that the system can function with a dynamic, non-linear holographic storage media. Complete reconstruction of a distorted input was not obtained, however, due to the 'single iteration' architecture implemented. The system demonstrated the ability to reconstruct one output image from several stored objects. Additional

reconstructions were not achieved due to the dynamic erasure of the holographic media during system operation. In all cases, the resolution of the output image was measured to be approximately 16 *l/mm*.

The inability of the system to generate a complete reconstructed image is addressed in the next chapter, which discusses implementation of a full resonant, closed loop HAM system.

V. *Resonant Cavity Holographic Associative Memory Using $Fe{:}LiNbO_3$*

5.1 Introduction

The previous chapter described experiments in which distorted objects were input into the single iteration HAM system, in the hope that fully reconstructed output images would be generated. While the single iteration system did, to a very limited degree, generate a more complete output image, the output could not be considered 'complete'. One possible explanation for this shortcoming is that the single iteration system does not generate a complete reconstruction of the original reference beam (used to store the hologram). Thus the hologram is not fully illuminated by the $BaTiO_3$ crystal's phase conjugate return. As a result, the output image is incomplete.

A system which allows multiple correlations of the object beam with the stored holograms should provide a more complete recreation of the reference beam, and hence generate an output image which more nearly matches the (complete) original object. Ideally, with each iteration, the system would 'fill in' a slightly larger area of the blocked input. Eventually, a complete reconstruction of the stored object would be produced.

In addition, typical optical neural network architectures which might use dynamic volume holographic media, such as $LiNbO_3$, are generally full resonant, closed loop systems. Examples of such optical cavities have been proposed by Wilson (31:73), Abu-Mostafa and Psaltis (1:89), Dunning et al. (7:209), and Lee et al. (17:162).

Pattern recognition systems which allow *complete* object recall from distorted or partial input objects and optical neural networks require the development of full resonant, closed loop holographic associative memories. This chapter describes

one possible full resonant architecture and reports on experimental results obtained during investigation of the multiple iteration system.

5.2 Optical Architecture

The architecture implemented for the full resonant holographic associative memory is an extension of the single iteration system investigated previously. The closed loop system is based on an architecture proposed by Dunning et al. (7:209).

The HAM consists of two optical 'legs', a reference leg and an object leg. Each leg has its own respective phase conjugate mirror. As in the single iteration system, a partial or distorted input object illuminates the holographic medium and generates the distorted reference beams. These beams are focused by the lens onto the first phase conjugate mirror, a 45 degree cut $BaTiO_3$ crystal. The crystal performs a non-linear threshold and phase conjugates (via self-pumped phase conjugation) the distorted reference beam. This wavefront then re-illuminates the hologram and generates a partially restored object wavefront. The partially restored object is focused onto the second PCM (another self-pumped 45 degree cut $BaTiO_3$ crystal) and is conjugated back towards the holographic medium. As this iterative process repeats, the output image continues to improve. As Dunning indicates, the closure of this full resonant loop is dependent on the losses present in the system. "If the combined gain of the PCMs is comparable to the losses in the cavity, oscillating wavefronts will build up which correspond to real and virtual images of the stored object having the largest correlation with the input object " (7:208). Figure 16 is a diagram of the full resonant HAM architecture investigated.

5.3 Experimental Results and Analysis

The procedures followed in the full resonant HAM cavity experiments are very similar to those used during the single stored object, single iteration system experiments. To begin, a hologram was recorded of the F-15, tank, and truck trans-

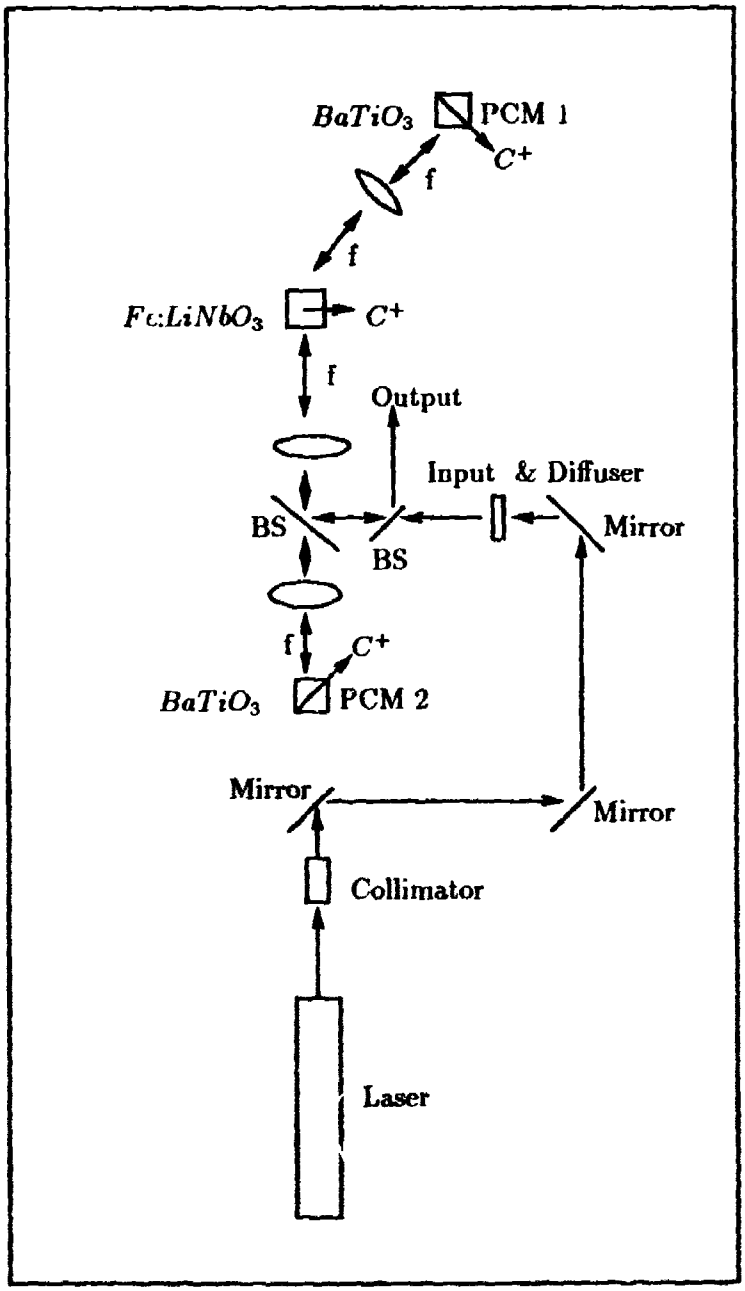

Figure 16. Resonant Cavity Holographic Associative Memory

parency used previously. The same plastic diffuser (as before) was attached to the object. The angle between the reference and object beams was held constant at thirty degrees. The normal to the c^+ axis of the iron doped lithium niobate crystal was located between the object and reference beams, six degrees from the reference beam. All beams were extraordinarily polarized. The recording process lasted for sixty seconds, at which time the reference beam was blocked and the diffraction efficiency measured. For all attempts at full resonant operation of the HAM system, the hologram diffraction efficiency ranged from three to seven percent.

The hologram was illuminated with an undistorted version of the stored object. A strong correlation beam was generated in the original reference beam direction. This beam, typically between 0.1 and 0.3 mW (initially), was focused onto the first PCM. Self–pumped phase conjugation began within the first three minutes. The power entering the PCM at this time was typically between 0.5 and 0.7 mW, again demonstrating the increasing diffraction efficiency of the hologram–diffuse object beam combination.

The phase conjugate return re–illuminated the hologram, generating the 'phase conjugate image'. This beam was incident on the first beam splitter (a 80–20 transmit to reflect ratio), and approximately 80 percent of the wavefront was focused onto the second PCM. The remaining 20 percent was reflected to the second beam splitter (a 70–30 transmit to reflect ratio). However, the thirty percent reflected by the second beam splitter, representing the output of the system, was too weak to be observed. In addition, the initial 80 percent incident on the second PCM amounted to a power of less than 0.01 mW. This beam was much too weak to allow a self–pumped phase conjugate return to be generated. Hence, closed loop, multiple iteration system performance was not achieved.

In an attempt to minimize beam power losses due to the beam splitters, the 70–30 beam splitter was removed. Since the output beam leaving this beam splitter was too weak to be observed, the beam splitter was serving no useful purpose. Thus,

removal would increase the original object beam power incident upon the hologram and create no detrimental effects on system diagnostics. With the second beam splitter removed, the maximum object beam power obtainable upon the hologram was approximately 30 mW.

A new hologram was written and the above procedure repeated. The initial hologram diffraction efficiency, calculated by illuminating the hologram with the 30 mW object beam and measuring the power diffracted towards the first PCM, was five percent. The 1.5 mW incident on the first PCM caused immediate beam fanning. A phase conjugate return was generated within the first 90 seconds. The resulting phase conjugate image incident on the second PCM was still too weak to form a phase conjugate return (0.02 mW). Based on the input object beam power, the hologram diffraction efficiency, and the beam splitters (and ignoring Fresnel surface reflection losses), the 0.02 mW power incident on the second PCM corresponds to a phase conjugate reflectivity from the first PCM of approximately 30 percent. While this reflectivity is less than the maximum achieved by Wilson (56 percent), it still represents a fairly high phase conjugate reflectivity (31:96). However, the low hologram diffraction efficiencies, coupled with the limited input object beam power and inevitable beam splitter loss, creates a fundamental limit to achieving full resonant system performance.

One last attempt at full resonant oscillation was performed by illuminating the hologram with the reference beam. While this procedure does not support an operational associative memory because the required correlations between stored objects and the distorted input are lost, it nevertheless serves to provide a much stronger beam entering the first PCM. As a result, more energy should illuminate the second PCM and perhaps allow resonant oscillation to occur. Unfortunately, even with 30 mW of power illuminating the hologram (and 95 percent of that incident upon the first PCM), only 0.3 mW of power was present at the second phase conjugate mirror. Previous experiments with the HAM system identified 0.5 mW as the approximate

minimum power required for self-pumped phase conjugation to occur in the two 45 degree cut $BaTiO_3$ crystals used in this experiment. Thus, even with the bright reference beam illuminating the hologram, losses in the system were sufficient to stifle full resonant oscillations.

Based on a 7 percent holographic diffraction efficiency, a 30 percent phase conjugate reflectivity of the first PCM, and a minimum power of 0.5 mW to initiate self-pumped phase conjugation in the second PCM, the architecture investigated would require an input object beam power of approximately 1.0 W. This estimate neglects losses due to Fresnel surface reflections and scattering within the holographic medium.

An alternative to merely increasing the incident object beam power (in order to support closed loop operation) would be to offset the cavity losses by means of signal gain. There are two areas where internal gain could be added to this architecture without detrimentally impacting system performance. Specifically, the phase conjugate mirror of the reference leg could be manipulated to provide gain to the phase conjugate return, and the phase conjugate return itself could be amplified by a separate photorefractive gain cell located in the reference leg. In addition, extreme care to provide a thermally and vibrationally stable environment during recording, coupled with the optimization of the recording parameters (based on the particular objects to be stored), should allow higher diffraction efficiency holograms to be written in the $Fe{:}LiNbO_3$ crystal. Chen et al. report diffraction efficiencies of up to 42 percent (4:224), while Amodei and Staebler have achieved diffraction efficiencies of 50 percent in thermally cycled holgrams (2:540). While this last item cannot be considered a separate 'gain' mechanism, it serves the same purpose by minimizing the significant signal loss due to low diffraction efficiencies.

In order to provide gain to the phase conjugate return generated by the reference leg PCM, the self-pumped phase conjugation technique currently used would have to be replaced by a four wave mixing scheme. Qualitatively, phase conjuga-

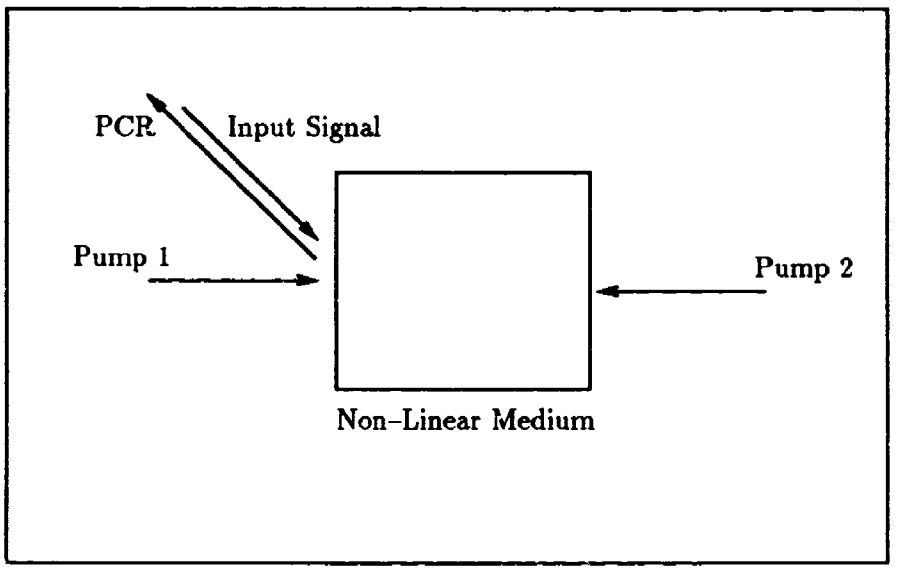

Figure 17. Traditional Four-Wave Mixing (FWM)

tion is pro ed by four wave mixing in a straight forward manner. A pump beam interferes with the incoming signal beam to form a grating. A second pump beam, contra-directional to the first pump beam, is incident on this grating and diffracts energy back towards the input signal beam. As a result, a 'phase conjugate' return is generated. If the power of this diffracted beam is greater than the incoming signal beam, the four wave mixing technique provides gain to the phase conjugate return. Figure 17 is a pictorial summary of optical phase conjugation by four wave mixing in a non-linear medium (18:549).

While four wave mixing complicates the architecture by requiring the presence of two carefully aligned pump beams, it nevertheless should provide the gain required for closed loop HAM operation. Assuming a seven percent holographic diffraction efficiency, a minimum power of 0.5 mW to initiate conjugation in the second PCM, and a 30 mW input object beam power, the four wave mixing would have to provide a gain of *at least* 4.2 to ensure closed loop operation. For these assumptions, approx-

imately 2.0 mW would enter the 'four wave mixer' and a phase conjugate return of 8.5 mW would emerge. The 8.5 mW beam would produce a beam of approximately 0.5 mW incident upon the second PCM. In actuality, the gain would have to be larger than 4.2 because Fresnel surface losses have not been considered. However, a gain of 4 to 5 is a reasonable first order approximation.

The second technique for providing gain to the reference leg signal involves the placement of an additional photorefractive crystal between the $Fe{:}LiNbO_3$ crystal and the first PCM's focusing lens, as indicated in Figure 18. This mechanism for providing the required gain was suggested by Dunning et al. (7:210), based on theoretical development of a 'Contra-Directional Two Wave Mixing' scheme produced by Yeh (34:323). This technique uses two wave coupling to provide gain to one beam at the expense of the other. The key difference between standard co-directional two wave coupling and contra-directional two wave coupling is the direction of the two input beams. In contra-directional two wave mixing, the two beams enter the crystal from opposite sides. Thus, this technique could possibly provide the gain required in the resonant HAM architecture. As Dunning et al. indicate,

> a two wave mixing photorefractive crystal operated in the counter propagating mode and located in the reference arm would impart a larger gain to the stronger reference component. By proper orientation of the crystal, the reference component propagating toward PCM 1 acts as a pump for the conjugated reference component propagating back toward the hologram. Since the two counter propagating reference components are conjugates of each other, their overlap in the crystal is maximized, which enhances energy transfer between them (7:210).

According to Yeh, the transmissivities of the two interacting beams are "formally identical to those of the co-directional two wave mixing" (34:326). Therefore, the gains obtained using contra-directional two wave mixing should be similar to those obtained using standard co-directional two wave mixing. Recent conventional two wave mixing experiments performed by Keppler have shown steady state gains of

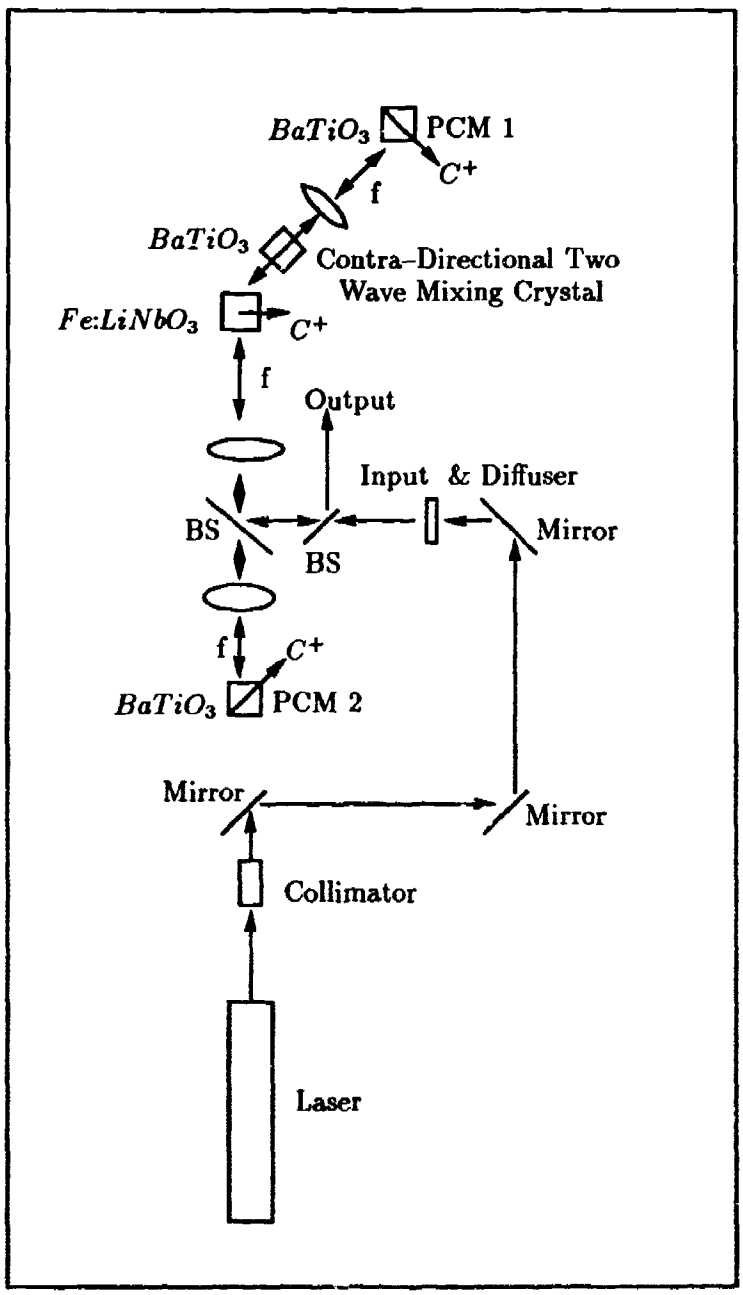

Figure 18. Resonant Cavity HAM with Internal Cavity Gain

up to 160 using 45 degree cut $BaTiO_3$ crystals (15). Assuming an input object beam power of 30 mW, a hologram diffraction efficiency of 7 percent, a 0.5 mW power requirement to initiate self-pumped phase conjugation in the second PCM, and assuming a self-pumped phase conjugate reflectivity from the first PCM of 30 percent, the gain required by a contra-directional two wave mixing amplifier would be approximately 14. Again, this value will necessarily be larger due to unaccounted Fresnel surface reflection losses, but it represents a valid first order calculation. From these calculations it appears that if contra-directional two wave mixing does indeed provide gains similar to conventional two wave mixing, the closed loop HAM system should successfully operate upon implementation of a contra-directional amplifier.

5.4 Conclusion

Attempts at using a full resonant, multiple iteration Holographic Associative Memory system to possibly enhance the *complete* recall of a distorted input were unsuccessful. Full resonant operation of the system was not achieved. Thus, the benefits expected from multiple correlations of the distorted input with the stored objects could not be realized. Without closed loop oscillations, the system operated as a single iteration HAM.

The inability of the HAM to operate in a closed loop fashion can be directly attributed to losses in the system. The problem was compounded by the relatively low input power (due to the internal étalon of the laser) and by the lack of gain in the system. Thus, the signal within the cavity diminished to the point that the beam incident upon the second phase conjugate mirror was below the power threshold required to form a conjugate return.

Three possible solutions to the problem were suggested. The first two dealt with means of providing gain to the signal within the cavity. A four wave mixing scheme which produces an amplified phase conjugate return was discussed, and first order calculations of the gain required to sustain closed loop operation were provided.

As a second alternative, 'contra-directional' two wave mixing was identified as a means of amplifying the reference leg phase conjugate return. Again, first order calculations of the required gain were provided. Lastly, the low diffraction efficiency of the iron doped lithium niobate holograms was identified as a major contributor to the losses in the cavity. Optimization of the writing of the holograms should support closed loop operation of the HAM by increasing the resulting diffraction efficiency and thus minimizing internal cavity losses. No suggestion was made to provide amplification in the object leg of the resonant cavity because, as Dunning et al. indicate, "the readout object may be distorted" (7:210).

Of course, the gains required for the four wave and two wave mixing schemes could be reduced if both techniques were used simultaneously. However, the complexity of the architecture would soon become unreasonable. The optimum choice would be to select and implement the mixing scheme which provides the largest useful gain, while also maximizing the holographic diffraction efficiency of the recording medium.

It should again be pointed out that alternative architectures have been proposed for optical neural networks and associative memory systems (reference the introduction to this chapter). These architectures are of the 'ring resonant cavity' variety. As a result, the signal beam does not travel back and forth upon itself (as in the architecture used in this research), but rather travels in a single, continuous direction. These systems do not depend on the generation of a phase conjugate return and can use conventional two wave mixing to provide the internal cavity gain required to sustain full resonant operation.

VI. Conclusions and Recommendations

6.1 Conclusions

This research effort investigated the use of a non–linear, dynamic holographic medium as the memory element in a holographic associative memory system. The theory of holographic storage in thick, photorefractive material was developed and experimentally demonstrated in support of an operational HAM. Specifically, holographic storage of two dimensional objects in iron doped lithium niobate was achieved. Initial experiments involved the optimization of recording parameters such as length of exposure, incident beam powers, crystal orientation, and beam polarization. Holographic diffraction efficiencies were found to increase with time during read out with the object beam. This unexpected result, which had not been previously reported, appears to be linked to the usage of a mild anisotropic diffuser in the object beam. The increasing diffraction efficiency resulted in a steadily increasing diffracted beam power and thus enhanced overall system performance.

The relevant theory defining operation of a single iteration HAM system using $Fe{:}LiNbO_3$ as the storage medium was developed. The mathematical model of a system in which multiple stored objects are illuminated with a particular distorted input, thus generating a complete reconstructed output image, were developed. Experimental implementation of the model verified basic system operation. Empirical observation of extraneous beams produced during system operation, coupled with subsequent supporting theoretical development, verified the presence of secondary (undesired) gratings within the holographic media. These additional gratings, caused by the air/lithium niobate refractive index boundaries creating internal reflections, could be eliminated by immersing the crystal in an index matching liquid gate. Distortion experiments partially demonstrated the system's capability to perform complete object recall. The reconstructed images were not entirely complete. It was felt that system performance was limited by the 'single iteration' architecture.

Multiple correlations of the reconstructed object beam with the stored objects are required before a complete output image will be constructed.

In order to achieve operation of the HAM system with multiple objects stored in the memory, experiments involving reference angle multiplexed holography were performed. Correct recording exposure was found to be critical to the storage of additional holograms while minimizing previous hologram erasure. Three separate objects were stored by varying the reference beam angle. Attempts to use the HAM to reconstruct any one image from its respective input object were successful. However, this process distorted the other two dynamic holographic gratings to such an extent that once one image was reconstructed, the other images could not be formed from the resulting diffracted light.

From the results, it appears that the 'one time' storage of multiple gratings is not sufficient to allow future reconstruction of any particular stored object. A system which cyclically re–writes the holograms after each 'read out' would be required. Another possible alternative would be to store the holograms permanently, thus removing the volatile nature of the medium. This alternative, however, eliminates the benefit of using dynamic media. In the case of optical neural networks, for example, permanent storage would not allow the system to 'learn' by continuous updating of the matrix weights contained in the holographic medium.

The last experiments investigated a full resonant, closed loop HAM system. It was hoped the multiple iterations provided by a closed loop system would allow *complete* object reconstruction. The architecture implemented, however, did not provide gain to the signal present in the cavity. As a result, the cavity losses were too large to allow resonant oscillations to occur. Three suggestions were made to alleviate this problem. The first two describe means to provide gain to the internal cavity signal by 1) replacing the reference leg's self–pumped phase conjugate mirror with a 'four wave mixer' which would generate an amplified phase conjugate return and by 2) placing a 'contra–directional' two wave mixing photorefractive crystal

in the reference leg. The third suggestion attempts to minimize cavity losses by optimizing the hologram recording process (and therefore maximizing the resulting diffraction efficiency).

6.2 Future Applications

In general, the HAM system can be used in applications where a conventional Vander Lugt type optical correlator is required. More specifically, permanent storage of multiple holograms in the non-linear medium, coupled with the inclusion of one of the two suggested gain mechanisms, should allow the full resonant HAM system to operate as a robust associative memory. Namely, distorted inputs would be processed by the HAM and result in *complete* output images. As an alternative to permanent holographic storage, a system which would utilize the dynamic nature of the medium by re-writing the stored holograms after each 'read cycle' should also allow implementation of the holographic medium as the memory element in an optical neural network.

6.3 Recommendations

Continued research with a HAM which uses dynamic holographic media should focus on the following areas:

1. Continued theoretical and experimental investigation of the anisotropic plastic diffuser used in this research to identify reason(s) for the unexpected increase in diffraction efficiency. Experiments with holographic recording, using just the diffuser as the object, should be performed to completely isolate the diffuser effects on holographic formation and reading. A detailed analysis of the paper by Staebler and Amodei (27) should be performed in order to identify the specific wave coupling mechanism(s) which are responsible for the increasing diffraction efficiency.

2. Investigation of permanent holographic storage in $Fe{:}LiNbO_3$, using thermally cycling techniques as described by Amodei and Staebler (2), to allow HAM operation with multiple stored objects. Permanent storage would eliminate the dynamic erasure problems encountered in this research.

3. Investigation of alternative dynamic holographic materials which provide 'real time' holographic recording and reading (such as $BaTiO_3$ and SBN (35:2094), GaAs, Inp and CdTe (12:2756), or $KNbO_3 : Fe^{2+}$ (8:163)).

4. Implementation of a spatial light modulator in place of the two dimensional object transparencies in order to eliminate the critical re-alignment required.

5. Investigation of the use of fractal grids (as described by Psaltis et al. (24:1755)) to improve reconstructed image quality by minimizing undesired cross-correlation noise.

6. Investigation of alternative architectures which allow continuous updating of the stored holograms, internal gain via conventional two wave mixing, and which do not require the generation of temporal phase conjugate beams (such as 'ring resonant' architectures).

7. Implementation of results obtained during this research in the development of an optical neural network.

Appendix A. *Secondary Grating Formation Within Fe:$LiNbO_3$*

A.1 Introduction

The equations describing the formation of a secondary grating in the Fe:$LiNbO_3$ crystal as a result of the coupling between the distorted input object beam, the phase conjugate return beam, and the original holographic grating are developed in this appendix.

A.2 Theoretical Development

Section 3.3 qualitatively described the formation of a second grating within the dynamic holographic medium. This grating, defined as T_p' below, is formed by the phase conjugate return (labelled $P_{c'}$), the distorted input object beam, and the original grating. The equations describing the formation and illumination of this second grating are developed for a single stored object. Additionally, to reduce the length of the equations, the directional phase terms $(\alpha f_y + \beta f_z)$ are rewritten in $\vec{k}$ notation. Thus, the key wavefronts and the original grating are defined as follows:

$$\vec{E}_r(f_x, f_y, f_z) = E_r \exp^{i(\omega t - \vec{k}_r \cdot \vec{f})} \tag{40}$$

$$\vec{E}_o(f_x, f_y, f_z) = E_o \exp^{i(\omega t - \vec{k}_o \cdot \vec{f})} \tag{41}$$

$$\vec{\hat{E}}_o(f_x, f_y, f_z) = \hat{E}_o \exp^{i(\omega t - \vec{k}_o \cdot \vec{f})} \tag{42}$$

$$\begin{aligned} T_p(f_x, f_y, f_z) \approx\ & 1 + i\gamma \left(|E_o|^2 + |E_r|^2 + E_o^* E_r \exp^{+i(\vec{k}_o - \vec{k}_r)\cdot \vec{f}} \right. \\ & \left. + E_o E_r \exp^{-i(\vec{k}_o - \vec{k}_r)\cdot \vec{f}} \right) \end{aligned} \tag{43}$$

$$\vec{P}_{cr}(f_x, f_y, f_z) = F\left[NL\left(F\left[i\gamma \hat{E}_o E_o^* E_r \exp^{i(\omega t - \vec{k}_r \cdot \vec{f})} \right] \right)^{\odot} \right] \tag{44}$$

where $\vec{f}$ consists of unit vectors in the f_x, f_y, and f_z directions, and $\vec{k}_o = \langle 0, 0, 1 \rangle$ and $\vec{k}_r = \langle 0, \alpha, \beta \rangle$. $\vec{E}_r$ is the original reference wave, $\vec{E}_o$ is the original object wave, $\vec{\hat{E}}_o$ is the distorted input object, T_p is the original holographic grating, and $\vec{P}_{cr}$ is the phase conjugate return.

T_p' is formed by the medium's response to the intensity of the total field:

$$T_p' \approx 1 + i\gamma' I' \tag{45}$$

where I' equals

$$\begin{aligned} I' &= \left|\hat{E}_o(f_x, f_y) + T_p(f_x, f_y) + P_{cr}(f_x, f_y)\right|^2 && (46) \\ &= |\hat{E}_o|^2 + |T_p|^2 + |P_{cr}|^2 + \hat{E}_o P_{cr}^* \\ &\quad + T_p P_{cr}^* + \hat{E}_o T_p^* + T_p^* P_{cr} + \hat{E}_o^* T_p + \hat{E}_o^* P_{cr} && (47) \end{aligned}$$

Dropping the (f_x, f_y, f_z) notation and the temporal terms, and performing several lines of algebra, generates the expression for T_p':

$$\begin{aligned} T_p' &= 1 + i\gamma' \left[|\hat{E}_o|^2 + |T_p|^2 + |P_{cr}|^2\right] \\ &\quad + i\gamma' \left(\hat{E}_o P_{cr}^* \exp^{-i(\vec{k}_o - \vec{k}_r)\cdot\vec{f}} + *\right) \\ &\quad + i\gamma' \left(P_{cr}^* \left[1 + i\gamma \left(|E_o|^2 + |E_r|^2\right)\right] \exp^{i\vec{k}_r\cdot\vec{f}} + *\right) \\ &\quad + i\gamma' \left(i\gamma P_{cr}^* E_o^* E_r \exp^{i\vec{k}_o\cdot\vec{f}} + *\right) \\ &\quad + i\gamma' \left(i\gamma P_{cr}^* E_o E_r \exp^{-i(\vec{k}_o - 2\vec{k}_r)\cdot\vec{f}} + *\right) \\ &\quad + i\gamma' \left(\hat{E}_o^* \left[1 + i\gamma \left(|E_o|^2 + |E_r|^2\right)\right] \exp^{i\vec{k}_o\cdot\vec{f}} + *\right) \\ &\quad + i\gamma' \left(i\gamma \hat{E}_o^* E_o^* E_r \exp^{i(2\vec{k}_o - \vec{k}_r)\cdot\vec{f}} + *\right) \\ &\quad + i\gamma' \left(i\gamma \hat{E}_o^* E_o E_r \exp^{i\vec{k}_r\cdot\vec{f}} + *\right) && (48) \end{aligned}$$

The '+ *' terms in the above equation indicate the addition of the spatial complex conjugate. The second grating is illuminated by both the distorted input beam and the phase conjugate return. The wavefronts leaving the grating as a result of the distorted input are described by the product of Equation 48 and Equation 42. Similarly, the wavefronts generated by the phase conjugate return are described by the product of Equations 48 and 44.

Bibliography

1. Abu-Mostafa, Yaser S. and Demetri Psaltis. "Optical Neural Computers," *Scientific American, 256:* 88-95 (March 1987).
2. Amodei, J. J. and D.L. Staebler. "Holographic Pattern Fixing in Electro-Optic Crystals," *Applied Physics Letters, 18:* 540-542 (June 1971).
3. Amodei, J.J. and D.L. Staebler. "Holographic Recording in Lithium Niobate," *RCA Review, 33:* 71-93 (March 1972).
4. Chen, F.S. et al. "Holographic Storage in Lithium Niobate," *Applied Physics Letters, 13:* 223-225 (October 1968).
5. Collier, Robert J. et al. *Optical Holography.* New York: Academic Press, 1971.
6. Dunning, G.J. et al. "All-Optical Associative Memory with Shift Invariance and Multiple-Image recall," *Optics Letters, 12:* 346-348 (May 1987).
7. Dunning, G.J. et al. "Optical Holographic Associative Memory Using a Phase Conjugate Resonator," *SPIE-International Society of Optical Engineering, 625:* 205-213 (1986).
8. Eichler, H.J. et al. *Laser-Induced Dynamic Gratings.* New York: Springer-Verlag, 1986.
9. Fielding, Capt Kenneth Henry. *A Position, Scale, and Rotation Invariant Holographic Associative Memory.* MS Thesis, AFIT/GEO/ENG/88D-2. School of Engineering, Air Force Institute of Technology (AU), Wright-Patterson AFB, OH, December 1988. (DTIC number not available at this time).
10. Fielding, Capt Kenneth Henry, et al. "A Position, Scale, and Rotation Invariant Holographic Associative Memory," *Optical Engineering, 28:* 849-853 (August 1989).
11. Gaylord, T.K. and F.K. Tittel. "Angular Selectivity of Lithium Niobate Volume Holograms," *Journal of Applied Physics, 44:* 4771-4773 (October 1973).
12. Gheen, Gregory and Li-Jen Cheng. "Optical Correlators with Fast Updating Speed Using Photorefractive Semi-Conductor Materials," *Applied Optics, 27:* 2576-2761 (July 1988).
13. Goodman, J.W. *Introduction to Fourier Optics.* New York: McGraw-Hill Book Company, 1968.
14. Gunter, P. "Holography, Coherent Light Amplification and Optical Phase Conjugation with Photorefractive Materials," *Physics Reports (Review Section of Physics Letters), 93:* 199-299 (January 1982).

15. Keppler, Capt Kenneth. *Optical Amplification with* 45 *Degree-Cut* $BaTiO_3$. MS Thesis, AFIT/GEO/ENG/89D-7. School of Engineering, Air Force Institute of Technology (AU), Wright-Patterson AFB, OH, December 1989. (DTIC number not available at this time).

16. Klein, M.B. et al. *Degenerate Four-Wave Mixing Smart Detector: Final Report*, February 1893 - May 1986. Contract MDA 904-83-C-0463. Maryland Procurement Office.

17. Lee, L. S. et al. "Continuous-Time Optical Neural Network Associative Memory," *Optics Letters, 14:* 162-164 (February 1989).

18. MacDonald, Kenneth R. and Jack Feinberg. "Theory of a Self-Pumped Phase Conjugator with Two Coupled Interaction Regions," *Journal of Optical Society of America, 73:* 548-553 (May 1983).

19. Magnusson, P. et al. "Holographic Interferometry Using Iron-Doped Lithium Niobate," *Applied Physics Letters, 51:* 81-82 (July 1987).

20. Mayo, 2Lt Michael W. *Computer Generated Hologram and Magneto-Optic Spatial Light Modulator for Optical Pattern Recognition.* MS Thesis, AFIT/GEO/ENG/87D-1. School of Engineering, Air Force Institute of Technology (AU), Wright-Patterson AFB, OH, December 1987. (ADA 189553).

21. Mayo, 2Lt Michael W. "Optical In-Plane Distortion Invariant Pattern Recognition in Structured Noise," *SPIE-International Society of Optical Engineering, 939:* 34-39 (April 1988).

22. Owechko, Y. et al. "Holographic Associative Memory with Nonlinearities in the Correlation Domain," *Applied Optics, 26:* 1900-1910 (May 1987).

23. Phillips, W. et al. "Optical and Holographic Storage Properties of Transition Metal Doped Lithium Niobate," *RCA Review, 33:* 95-109 (March 1972).

24. Psaltis, Demetri et al. "Adaptive Optical Networks Using Photorefractive Crystals," *Applied Optics, 27:* 1752-1759 (May 1988).

25. Shah, Pradeep et al. "Volume Holographic Recording and Storage in Fe-Doped $LiNbO_3$ Using Optical Pulses," *Applied Physics Letters, 24:* 130-131 (February 1974).

26. Smith, Howard M. *Principles of Holography.* New York: John Wiley & Sons, 1975.

27. Staebler, D.L. and J.J. Amodei. "Coupled-Wave Analysis of Holographic Storage," *Journal of Applied Physics, 43:* 1042-1049 (March 1972).

28. Staebler, D.L. et al. "Multiple Storage and Erasure of Fixed Holograms in Fe-Doped $LiNbO_3$," *Applied Physics Letters, 26:* 182-184 (February 1975).

29. Weaver, John Elbert. *Angular Addressing Properties of Volume Fourier Transform Holograms in Iron-Doped Lithium Niobate.* PhD dissertation. School

of Electrical Engineering, Georgia Institute of Technology, February 1979 (ON7913851).

30. Weaver, J. E. and T.K. Gaylord. "Evaluation experiments on Holographic Storage of Binary Data in Electro–Optic Crystals," *Optical Engineering, 20:* 404-411 (May/June 1981).

31. Wilson, Jeffery A. *Optical Information Processing in a Confocal Fabry–Perot Resonator.* MS Thesis, AFIT/GEO/ENG/88D-5. School of Engineering, Air Force Institute of Technology (AU), Wright–Patterson AFB, OH, December 1988. (DTIC number not available at this time).

32. Wood, Elizabeth A. *Crystals and Light: An Introduction to Optical Crystallography.* New York: Dover Publications, Inc, 1977.

33. Yariv, Amnon and Pochi Yeh. *Optical Waves in Crystals.* New York: John Wiley & Sons, 1984.

34. Yeh, Pochi. "Contra–Directional Two–Wave Mixing in Photorefractive Media," *Optics Communications, 45:* 323-325 (May 1983).

35. Yeh, Pochi et al. "Optical Interconnection Using Photorefractive Dynamic Holograms," *Applied Optics, 27:* 2093-2096 (June 1988).

Vita

Dwayne W. Frye was born on 13 March 1962 in Gary, Indiana. He graduated from Portage High School in Portage, Indiana in 1980. He attended Purdue University where he earned a Bachelor of Science in Electrical Engineering. Upon graduation, he entered the USAF Officer Training School and was commissioned a Second Lieutenant in August, 1984. Capt Frye's first assignment was to the Rome Air Development Center (RADC), Griffiss AFB, New York, where he served as a research engineer and program manager in the Surveillance Directorate, Advanced Electro-Optic Technology Division. Capt Frye earned a Masters in Business Administration in Management from Rensselaer Polytechnic Institute while stationed at Griffiss AFB. In May 1988, he entered the Electro-Optics Masters Program in the School of Engineering, Air Force Institute of Technology.

Permanent address: 5076 Concord Ave
Portage, Indiana 46368